Development of a comparative test methodology to characterize scratch and stickiness of PP-compounds

Master's Thesis

of

Umut Doğar ÇAKMAK

performed at

Polymer Competence Center Leoben GmbH

and

BOREALIS Polyolefine Linz GmbH

Academic advisor: O.Univ.-Prof. Dipl.-Ing. Dr.mont. Reinhold Lang
Dipl.-Ing. Dr.mont. Zoltán Major

Industry advisor: Dipl.-Ing.(FH) Georg Grestenberger

Assessor: Ao.Univ.-Prof. Dipl.-Ing. Dr.mont. Gerald Pinter

February 2010

ACKNOWLEDGMENT

I would like to thank Ao.Univ.-Prof. Dipl.-Ing. Dr.mont. Gerald Pinter for assessing my thesis.

It is a pleasure to thank those who made this thesis possible, O.Univ.-Prof. Dipl.-Ing. Dr.mont. Reinhold W. Lang and Dipl.-Ing. Dr.mont. Zoltán Major, whose encouragement and guidance from the initial to the final level enabled me to develop an understanding of the subject.

The research of this current Master's thesis was performed during my employment as Junior Researcher at Polymer Competence Center Leoben GmbH. For the successful proceeding of the work, I would like to thank my industry advisor Dipl.-Ing.(FH) Georg Grestenberger. We had insightful conversations during the development of the ideas in this thesis.

I offer my regards and blessings to all employees of BOREALIS Polyolefine Linz GmbH, who supported me in any respect during the completion of the project.

My girlfriend Felicitas Hügel has been an inspiration throughout my whole study. She has always supported my dreams and aspirations. Finally, I would thank my parents Ahmet and Telli for enabling my student's life and if I do say so myself, I think they did a fine job raising me.

The research of the Master's Thesis was performed within the framework of the project III.3.02 at the Polymer Competence Center Leoben GmbH (PCCL, Austria) as a member of the $\mathbf{K}_{plus}$-program of the Austrian Ministry of Traffic, Innovation and Technology with contributions by BOREALIS Polyolefine Linz GmbH. The PCCL is funded by the Austrian Government and the State Governments of Styria and Upper Austria

OUTLINE

ABSTRACT

Generally, sticky surfaces are characterized by adhesiveness. However, it is undesirable to touch on sticky surfaces of any products such as automobile instrument panels and interior trims. The major focuses of this present work were on both the development of an objective stickiness measurement and the surface characterization of thermoplastic polyolefin (TPO)-compounds for automotive interior applications. This laboratory stickiness test should complete the current surface characterization tests at BOREALIS Polyolefine Linz GmbH, which includes scratch visibility and gloss measurement. The major elements of this stickiness test are the compression/tension loading, the standardized counterpart (modulus, surface roughness) and the controlled duration of the test. Different model TPO formulations developed and produced by the company partner were used for these investigations. Since the stickiness phenomenon is assumed to be a reason of the degradation of anti-scratch additives (slip agents) after UV irradiation, the model TPOs were formulated with varying amount and type of ready-made anti-scratch additives. The objective of this thesis was to examine the hypothesis that the stickiness occurrence is caused by slip agents with the help of the stickiness test methodology, as well as to verify the correlation of the stickiness test to the human sense of touch. To capture the influence of material conditioning, the materials were tested both in the unconditioned state and after various intervals of UV irradiation in an environmental chamber. The artificial UV irradiation was defined by the Kalahari condition (typical for automotive applications), where the materials were faced to a Xenon arc light source in a dry and hot climate.

First of all, it has been shown that the stickiness test is reliable, reproducible, easy to implement and flexible in terms of materials' pretreatment. Based on the results of all experiments, the best material formulation for a balanced stickiness-surface appearance-cost performance was found. Basically, the results of scratch and stickiness characterization indicate that the slip agents are not the main influencing factor for the occurrence of sticky touch on TPO surfaces. It is rather a complex interaction with other additives (e.g., UV stabilizer, antioxidants) during UV irradiation induced degradation of slip agents. The last aspect is to be clarified in further studies.

KURZFASSUNG

Klebrige Oberflächen werden durch ihre Adhäsivität charakterisiert. Bei vielen Produkten wie z. B. Automobilinstrumententafeln und -innenraumverkleidungen sind klebrige Oberflächen nicht erwünscht. Die vorliegende Arbeit beschäftigte sich sowohl mit der Entwicklung einer objektiven Messmethode für die Oberflächenklebrigkeitsmessung (Stickiness), als auch der Oberflächencharakterisierung von thermoplastischen Polyolefin (TPO)-Compounds für Automobilanwendungen. Diese Labor-Stickiness-Prüfung sollte die aktuellen Oberflächencharakterisierungstests bei der BOREALIS Polyolefine Linz GmbH, welche die Kratzfestigkeits- und die Glanzmessung prüfen, ergänzen. Die Hauptmerkmale dieser Stickiness-Prüfung sind die Druck-/Zugbelastung, die standardisierte Gegenfläche (Modul, Oberflächenrauheit) und die definierte Durchführung des Tests. Es wurden unterschiedliche TPO Modellrezepturen, die vom Firmenpartner entwickelt und hergestellt wurden, untersucht. Es wird angenommen, dass für das Auftreten des Stickiness-Phänomens nach UV-Bestrahlung der Materialien, degenerative Abbauprodukte der Anti-Scratch-Additive (Gleitmitteln) verantwortlich sind. Daher wurden die Modell TPO-Werkstoffe mit unterschiedlichen Mengen und Typen von gebrauchsfertigen Anti-Scratch-Additiven formuliert. Ziel dieser Arbeit war es, die Hypothese, dass das Auftreten von Stickiness durch Gleitmittel verursacht wird, mit Hilfe der Stickiness-Testmethode zu überprüfen und die Korrelation des Stickiness-Tests mit dem menschlichen Tastsinn zu validieren. Um den Einfluss der Materialkonditionierung zu erfassen, wurden die Materialien sowohl im unbehandelten Zustand, als auch nach verschiedenen UV-Bestrahlungsintervallen in einer Laborbewitterungskammer getestet. Die künstliche UV-Bewitterung wurde durch die Kalahari Klimaverhältnisse – trockenes und heißes Klima – definiert (typisch für Automobileanwendungen), wo die Materialien durch eine Xenon-Lichtquelle bestrahlt wurden.

Zunächst hat sich gezeigt, dass der Stickiness-Test zuverlässig, reproduzierbar, einfach zu implementieren und flexibel in Bezug auf Materialienvorbehandlung ist. Gleichzeitig ist es auf der Basis der gemessenen Ergebnisse möglich, das beste Material mit einer ausgewogenen Stickiness-Oberflächenerscheinung-Kosten-Leistung zu bestimmen. Grundsätzlich zeigen die Ergebnisse von Kratzfestigkeits-

und Stickinessmessungen, dass die Gleitmittel nicht der wichtigste Einflussfaktor für das Auftreten von Stickiness an TPO-Oberflächen sind. Es ist eher eine komplexe Interaktion der Gleitmittel mit anderen Additiven, wie z. B. UV-Stabilisatoren und Antioxidantien, induziert durch die UV-Bestrahlung. Letzterer Aspekt ist in weiterführenden Untersuchungen aufzugreifen und zu klären.

1 INTRODUCTION

Each original equipment manufacturer (OEM, e.g., VW, BMW etc.) in the automotive industry requires polypropylene (PP)-compounds for interior products according to their own material's specifications. These specifications require a property spectrum of the material after processing, including:

- Mechanical properties (e.g., stiffness, impact strength, brittle-ductile transition temperature etc.)
- Thermal properties (e.g., heat deflection temperature, coefficient of linear thermal expansion, thermal conductivity etc.)
- Purity (e.g., fogging, odor etc.)
- **Surface properties**

The focus of this research is on the required surface properties, which include high scratch resistance, good haptics (e.g., no sticky touch), and low gloss. Thereby, material suppliers of PP-compounds for such applications incorporate different additives to a base resin to fulfill these requirements. However, in some cases OEMs observe stickiness on product's surface, which is assumed to be a consequence of the anti-scratch additives. In the present literatures [1; 2; 3] were also reported, that after weathering the surfaces of PP-compounds were becoming a sticky touch. This occurrence was partly assessed and the deduced hypothesis of the results was that anti-scratch additives were responsible for this phenomenon.

However, driven by the literature and the before mentioned observation of several OEMs, the objective of this thesis is to examine and to verify the hypothesis by varying of incorporated anti-scratch additive types, and to investigate the best additive-surface appearance-cost performance within the scope of OEM requirements. Since the stickiness phenomenon is related to weathering conditions, the material's examination is to perform after various intervals of weathering (UV irradiation intensity, temperature, humidity and time).

The state-of-the-art assessments of stickiness are, in general, internal standards using a ranking system based on a specific definition of stickiness [4] or a subjective comparison of a specimen to a reference [5]. So, there is no objective and reliable stickiness test method established. Hence, it is necessary to develop and implement a physically founded measurement methodology – primary – to examine the hypothesis and – secondary – to complete the need of industry for such a test. Furthermore, the results of this stickiness measurement methodology should correlate to the human sense of touch. To support this method development efforts several model thermoplastic polyolefin (TPO) materials were developed, produced and injection molded by BOREALIS Polyolefine Linz GmbH for these investigations.

2 BASIC CONSIDERATIONS

The objective of this chapter is to highlight the important background of material behavior for understanding the surface properties of automotive interior components. Based on these fundaments the main factors for a long-term decreasing of surface appearance limited by OEM-requirements will be discussed.

2.1 Thermoplastic Polyolefin and Effects of Surface Modifier Additives

Polyolefin blends, such as thermoplastic polyolefins (TPOs), are based primarily on ethylene-propylene random copolymer (EPM) and isotactic polypropylene (iPP) and represent an important family of engineering materials [6]. PP, as the matrix phase constituent, is low in cost and has a low density [6]. Its crystalline structure and relatively high crystalline melting point, depending on grade, in the range of 145 °C to 165 °C, give it resistance to oil, solvents, and elevated temperature [6]. Elastomers of ethylene-propylene-diene terpolymer (EPDM) and EPM types are logical choice for the elastomeric phase because of their thermal stability, low cost, flexibility at low temperatures, and structural similarity to PP [6]. This similarity also means a good compatibility in blending [6]. Furthermore, advances in Ziegler-Natta and metallocene catalysis allow copolymerization of an elastomeric soft component in a shell or skin of crystalline PP [6]. Such products are referred to as reactor thermoplastic polyolefins (RTPOs) [6].

Products made of TPOs cover a wide range of properties that essentially bridge the gap between soft rubber and engineering plastics [6]. They can be formulated to combine strength and toughness with properties from soft traditional rubber to relatively stiff products with high impact strength [6]. With increasing amount of the elastomeric phase the tensile strength and the Young's modulus decreases. However, both the notched and unnotched impact strength increases, and the tensile impact strength goes through a minimum following an increasing [7]. In general, the impact strength depends on the average particle size and particle size distribution of the elastomeric phase, the phase viscosity ratio, and the average spherulite size and crystallinity of the matrix phase [7]. Thereby, multiple crazing and shear yielding are

responsible for the impact energy dissipation [7]. In TPOs shear yielding takes place above room temperature, which is caused by the glass transition temperature T_g of PP [7]. In addition, the occurrence is favored by very fine and narrow dispersion of the impact modifier [7]. Due to this property profile, TPOs gained wide acceptance for applications in the automotive industry, among other industries [8]. These materials are often molded into decorative or protective interior and exterior parts [8]. However, it was shown that TPOs exhibit relatively poor scratch resistance as compared to other engineering plastics or types of materials [8]. Consequently, for many applications the scratch resistance/visibility of materials needs to be improved in order to fulfill the customer requirements [8]. For further information it is referred to [6; 7; 8].

Surface effective modifier

A successfully employed way to reduce scratch damage in PP based materials is to lubricate the surface using slip additives [3]. Slip agents can be categorized as

- Migratory slip agents and
- Nonmigratory slip agents [3].

Generally, the lubrication of these slip agents leads to a reduction of the coefficient of friction (COF), so the magnitude of the maximum stresses during scratching are also decreased, which in turn reduces brittle scratch damage such as cracking [3]. A further consequence of a reduced COF is a decreased yielding zone size during scratching [3]. As a result of these, the scratch visibility is decreasing [3].

To lubricate the surface the **migratory slip agents** have to migrate from the bulk material [3]. The main advantages of these additives are their effectiveness in decreasing the COF at the surface and excellent cost performance, in general [3]. Primary and secondary fatty amides are the most common migratory slip additives, which includes oleamide, erucamide, stearyl-erucamide, ethylene-bis-stearamide etc. [3]. As examples for migratory slip agents in Figure 2.1 are oleamide and erucamide illustrated. A consequence of their migratory nature is that they may require some time after molding to form a lubricating layer on the surface [3]. The required time depends on the concentration and molecular mass of the additive, the thickness of the prod-

uct, the nature of the polymer substrate, and the influence of other formulation constitutive as well as ambient temperature [3]. In nonpolar polymers, such as polyolefins, the lubricating layer is very weakly bound to the polymer surface and can be disrupted by exposure to humidity and heat as well as physically wiping the surface [3]. Therefore, the slip agents have to migrate continually to provide a long-term surface protection and hence an enduring surface appearance [3]. The effect can be achieved by depositing multiple layers of slip agent at the surface or by introducing polar functionality to the polymer surface to enable a stronger interaction with the polar amide of the slip agent [3]. However, at some point during the lifetime of a product all of the slip agent will be exhausted [3]. Consequently, the scratch resistance of a TPO product alters during the lifetime too [3]. Furthermore, it is observed that sometimes products surface are sticky after weathering, which is suspected to be caused by the migratory slip agents [1; 2; 3].

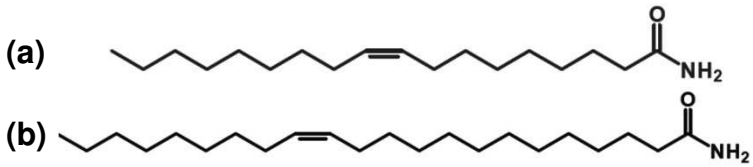

Figure 2.1: Two state-of-the-art migratory slip agents; **(a)** oleamide (9-cis-octadecenamide), **(b)** erucamide (13-cis-docosenamide).

On the other hand, **nonmigratory slip agents** are by their nature randomly distributed throughout the material and have to be used at higher concentration as their counterparts to be present sufficiently at the surface [3]. The most common nonmigratory slip agents are high molecular mass polysiloxanes [3]. These types of additives provide an immediate and the material surfaces are slightly more durable scratch resistant compared to migratory slip agents [3]. Main disadvantages are the high price and the higher concentration, which is necessary to give an effect at the surface [3]. Furthermore, polysiloxanes are prone to adsorption on talc filler. Therefore, a pretreatment of the talc is required to enhance an effective surface lubrication [3].

2.2 Scratch Behavior of Polymers

Abrasion and wear is a phenomenon occurring when two moving surfaces are in intimate contact [9]. It is generally believed that asperity interactions between these moving surfaces are responsible for such occurrence [9]. The involved mechanisms include adhesion, shearing, fatigue, micro-cutting and surface smearing [9]. As compared to other materials the situation for polymers is more complicated, which is caused by their viscoelastic-viscoplastic nature [9]. Due to this property, wear features alter with the history of wear and time of observation [9]. Furthermore, polymers are relatively soft and so more prone to scratches and abrasion [9]. Since abrasion and wear can be considered as multiple asperities making multiple and repeated scratches on the contact surface, a simplified situation where a stylus is used to scratch a polymer surface is often examined to gain insight into this complex process [9].

2.2.1 Terminology

In general, a distinction is made between marring and scratching to summarize the many ways of mechanically damaging a surface with a device (e.g., stylus) [10]. Thereby, marring occurs under less severe conditions compared to scratching [11]. Consequently, **mar resistance** is the ability of a material to resist surface damage from light abrasion by small objects [12]. It is often associated with a high density of small, shallow scratches distributed over a relatively large area that larger scale appearance characteristics are affected [11]. Mar resistance can be measured by the loss in gloss, increase in haze or shift in gray level [12]. On the other hand, **scratch resistance** is the ability of a material to withstand damage that is accompanied by the gross deformation typically associated with sharp objects [12]. Contrary to marring it is associated with a much lower density of larger, deeper scratches – also single scratches – where the size of the scratch is visual perceivable [11]. For applications where surface aesthetics are important the **scratch whitening/visibility** is a key phenomenon, which is a result of the scattering of light from the surface [12; 13]. It is defined as the visible damage along the scratch groove of the surface caused by micro-cracking, voiding, crazing and debonding [12; 13].

2.2.2 Scratch Damage Mechanisms and their Dependencies

The described scratch process is defined as a mechanical deformation process where a force or displacement controlled stylus penetrate and moves along the surface at a prescribed velocity (see Figure 2.2) [14]. The indentation process involves a strong shear-compression stress field and the sliding process is a shear-stress dominant process [13]. Therefore, the high shear stresses, which are involved in the scratch process, lead to a distortional deformation dominant mode [13].

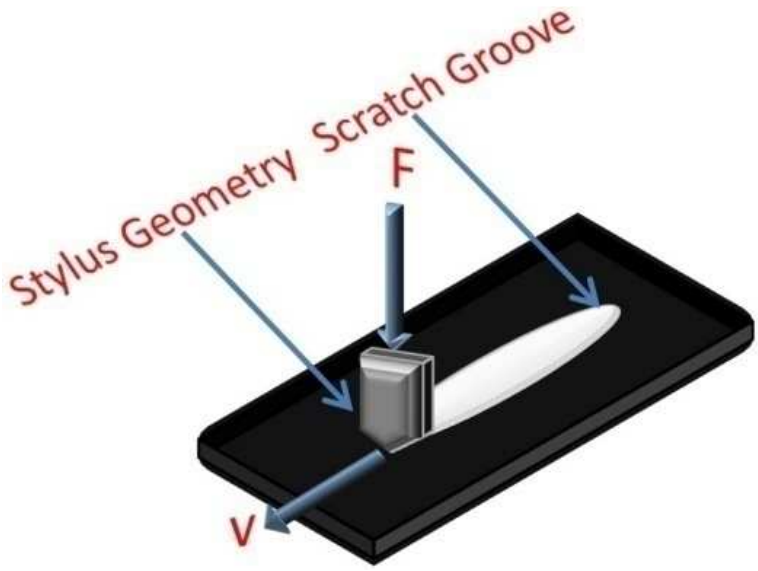

Figure 2.2: Schematic illustration of the scratching process.

Polymeric materials are viscoelastic-viscoplastic in nature. From this it follows that polymers have, in general, both a test and an environment conditions dependent material behavior [9; 10; 11]. In terms of scratch performance and resulting damage feature of a polymer can be significantly affected by

- Experimental conditions (i.e., loading, velocity and temperature),
- Stylus geometry (e.g., spherical, conical) and
- Intrinsic material characteristics [9; 10; 11].

Generally, depending on these constitutive factors, material damage feature can occur as a ductile damage (e.g., shear yielding and ironing, which means a smoothing of local asperities) or a brittle damage (e.g., crazing and cracking) [11; 14]. Addition-

ally, debonding and voiding can occur if the polymer contains inclusion phases, such as talc and rubber (e.g., TPO) [14].

Under a linear increase of the magnitude of **loading**, sudden changes in frictional force – consequently the coefficient of friction (COF) – normally indicate the initiation of fracture, changes in scratch features and changes in deformation mode of polymers [9]. In which polymers might recover elastically without scratch marks after scratching below a critical load and depending on material characteristics [9]. As frictional behavior of surfaces is a function of applied force, it affects the stress magnitude and the distribution during scratching of polymers [9]. There are differences in macro- and micro/nano-scale for some polymers (e.g., polystyrene PS) [9]. Thereby, the frictional force increase with applied force, the COF is constant in macro-scale, but when light load is applied to produce nano-scratch the COF is not constant and in many cases lower than macro-friction [9]. This is suggested to be caused by a reduction of real contact area [9].

The importance of scratching **velocity** lies in the ability to change the strain – strain rate – at the interface of the specimen and the stylus and thus changes the deformation mode of polymers [9]. Especially for nano-scratches, the relationship between velocity and COF depends on the relaxation state (displacement controlled) of the affected surface [9]. An increase in scratch velocity that accompanies the high groove force will produce a substantial friction heat exchange at the contact [9]. Such heat may facilitate the permanent displacement of the material [9].

When **temperature** is increased, the stylus penetrates deeper into the material and the contact area between stylus and specimen increases due to thermally induced softening of polymers [9]. Furthermore, the increase in temperature may lead to an increase in the contribution of viscous energy loss of the friction of polymers [9].

There are also situations, where the fluctuations in loading curves during scratching, were associated with slip-stick phenomenon and crack growth [9; 14]. In the case of slip-stick motion, both true force and true scratch velocity experienced by the polymer will change with scratch distance [9; 14]. If this phenomenon occurs during scrat-

ching, the scratch velocity and temperature influence the amplitude, period and average horizontal force of the process [9; 14].

Scratch damage mechanism is extremely dependent on contact geometry, in general [9; 11]. Particularly the **stylus** included/attack angle and tip radius are the main **geometry** parameters, which influence the scratch damage mechanism of polymers [9; 11]. The higher the attack angle is the severe is the deformation and so producing increasingly brittle damage modes [9; 11]. The difference between maximum shear stress in front of a stylus and the maximum tensile stress behind is crucial to determine the deformation mechanism during scratching [9; 11].

The **intrinsic material characteristics**, such as Young's modulus and yield strength, influence the size of deformation zone, amount of recovery and deformation mode [9; 10]. Also, depending on modulus and yield strength of polymers, the radius of contact zone, the penetration depth and plastic zone size will vary [9; 10]. However, each change of materials characteristics (e.g., molar mass distribution) to influence the mechanical properties will impact on both scratch resistance and deformation mode [9; 10]. There are possibilities of

- Modifying the polymer molecular structure (e.g., crystallinity),
- Blending polymers and
- Producing polymer composites with various fillers and additives

to improve the tribological properties of a given polymeric material [10]. Xiang et al. [13] summarized, based on their investigation, a qualitative relationship between the scratch visibility, as an indicator for scratch resistance, and material characteristics (see Figure 2.3) [13]. The occurrence of brittle fracture during scratching is often associated with increasing scratch visibility compared to scratches for which viscoelastic and/or viscoplastic damage occurs [11]. Furthermore, the scratch visibility can also be affected by the color of the specimen, relative orientation of incident light, scratch direction and the observation time after scratching [11; 15].

It should be highlighted for strengthened and toughened polymer blends (e.g., TPO) that mode II fracture toughness might be related to shear-induced fracture during scratching. As this type of polymers can have weak bonding between the dispersed phase and the matrix [13]. Consequently, debonding and cracking may be easily generated by internal sliding friction in the shear-stress dominant region of the scratched polymer subsurface [13]. When talc is incorporated to strengthen the polymer, the inherent white color of talc can increase scratch visibility due to light reflection from exposed talc particles [8].

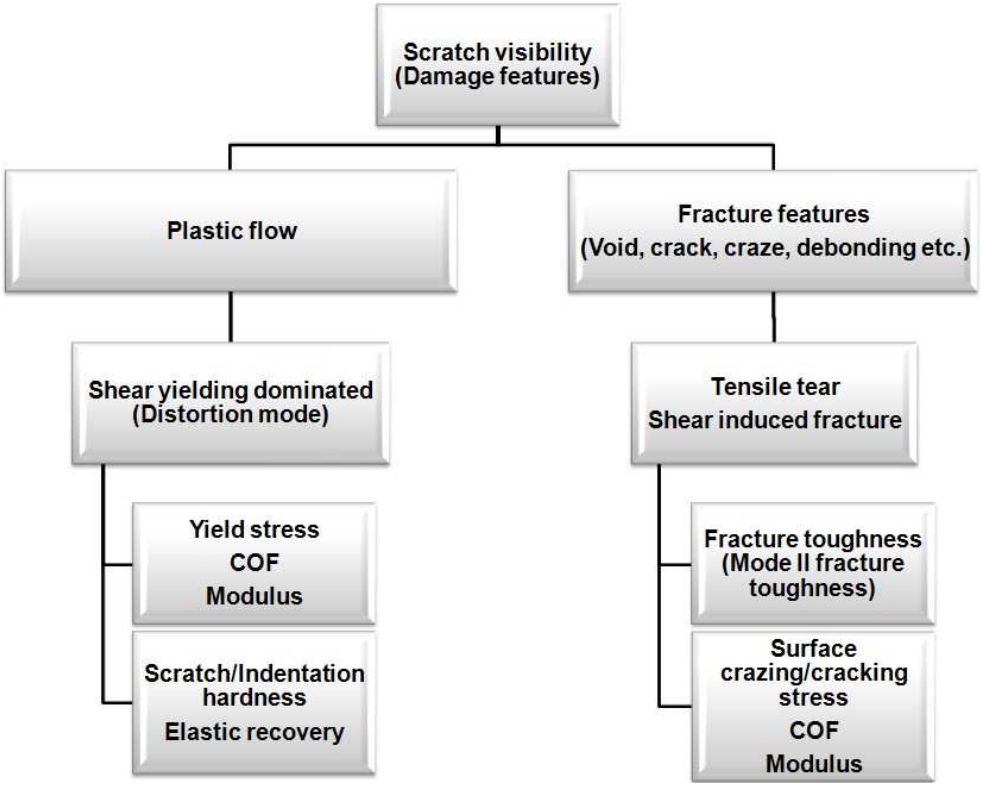

Figure 2.3: The Flow chart is showing the relationship between scratch visibility and material characteristics. **[13]**

The deformation during scratching of a polymer progresses according a function of the severity of contact conditions, such as loading, velocity etc. from elastic deformation to ironing, viscoelastic-viscoplastic ploughing, ductile machining, followed by cracking, and finally brittle machining [9; 11]. In this case machining does mean chipping of the material [9; 11]. These deformation processes are highly dependent on contact geometry and penetration depth [9; 11]. An increasing temperature enhances

viscoelastic-viscoplastic ploughing responses while a decreasing for elastic and brittle responses [9; 11].

Figure 2.4 shows scanning electron (SEM) micrographs of an unfilled PP, a PP with talc, and a PP with talc and lubricant. These materials were investigated by Chu et al. [15] with the aid of the Ford Lab Test Method for scratching the materials' surfaces. The micrographs were taken from 7 N scratch test specimens. These pictures show how the scratch damage of PP alters with incorporation of talc and lubricant. In the PP with talc material (see Figure 2.4 **(B)**) multiple cracks at the boundary (scratched-unscratched), plastic deformation, voids and some debonding were observed [15]. On the other hand, in the PP with talc and lubricant material (see Figure 2.4 **(C)**) more cracks and extensive plastic deformation were found [15]. In addition, different types of scratch morphologies are schematically illustrated in Figure 2.4 **(D)** [9].

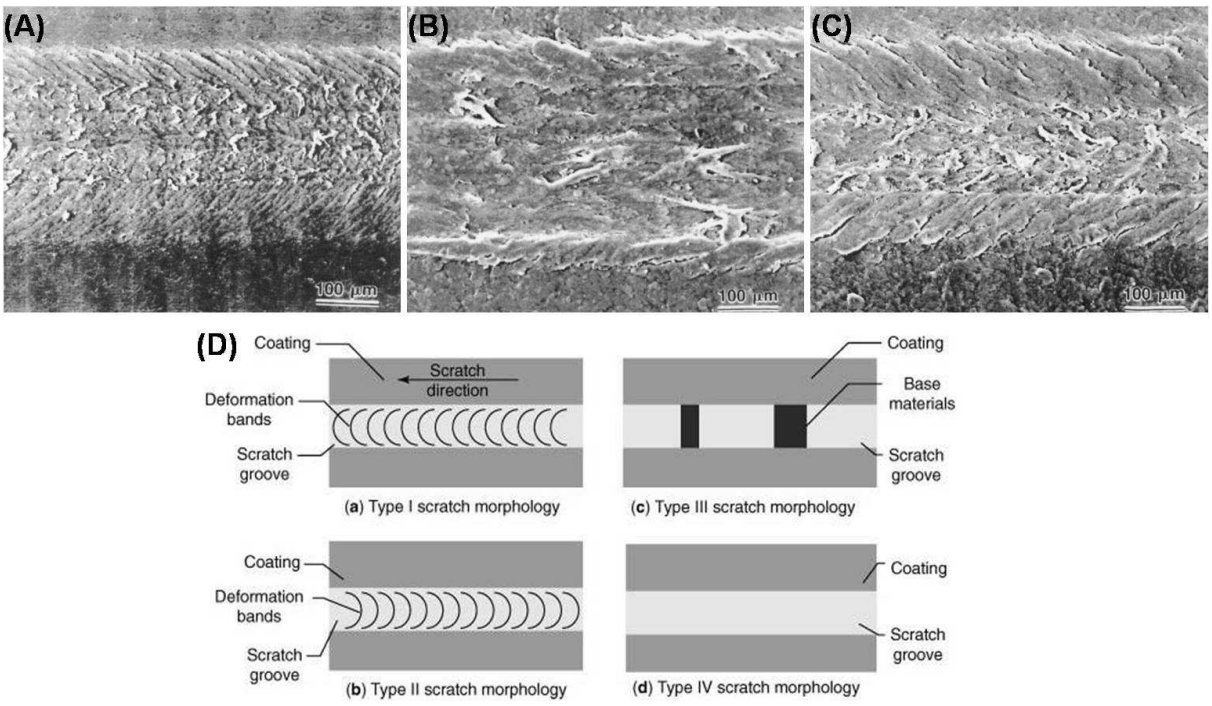

Figure 2.4: Demonstration of the scratch damages' SEM micrographs **(A)**, **(B)** and **(C)** of an unfilled PP, a PP with talc, and a PP with talc and lubricant, respectively **[15]**; The scratch direction for **(A)**, **(B)** and **(C)** is from left to right. **(D)** is illustrating schematically the different types of scratch morphologies; Type I ➔ ductile materials (fish-scale), Type II ➔ brittle materials (parabolic crack), Type III ➔ delamination, and Type IV ➔ plastic ploughing **[9]**.

Jiang et al. [14] observed scratch damage features, such as mar, fish-scale, parabolic crack, and materials removal for general types of polymers after scratching according to ASTM and ISO test standards. The scratch damage features for TPOs, which will be discussed in detail, are illustrated in the second row – weak ductile – of the scratch damage evolution map in Figure 2.5 [14]. The other material types, which were investigated in [14], were polycarbonate PC (ductile and stronge), polystyrene PS (brittle and weak) and Epoxy (brittle and strong).

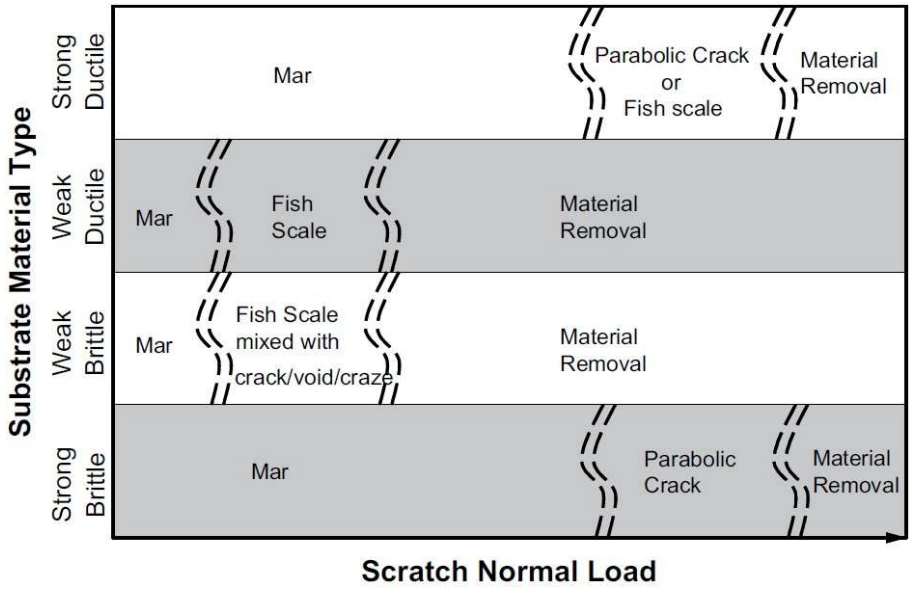

Figure 2.5: Scratch damage evolution map for general types of polymers. **[14]**

For polymers, which have low tensile strength and high ductility (e.g., TPO), mar damage will occur first under a low scratch load [14]. With increasing scratch normal load, the TPO begins to undergo plastic deformation, forming a periodic concave damage feature pointing toward the scratch direction [14]. This ductile damage mode is called fish-scale damage and is one of the most widely observed phenomena for polypropylene based polymers [8; 14]. Hence, the previous described slip-stick phenomenon during polymer scratching is observed to be responsible for the fish-scale damage feature. With further increase in scratching load magnitude, material removal takes over to rupture the well-developed fish-scale feature [14]. Finally, significant material removal occurs from the surface [14].

2.3 Stickiness

Associated with migratory slip agents, such as the state-of-the-art additive erucamide, it was reported for some scratch resistant TPO-formulations to become a sticky touch after exposure to natural or accelerated weathering (e.g., Kalahari, Arizona etc.) [2; 3].

In general, the amide slip agents contain carbon-carbon double bonds [3]. Particulary, the allylic carbon atoms adjacent to these C=C bonds are vulnerable to thermal- and photo-oxidation [3]. During weathering, where these oxidations will initiate, the products of oxidation appear to be responsible for the stickiness of the surface [3]. As weathering continues, the oxidation products also continue to degrade to lower molecular mass species until they are vaporized from the product surfaces [3]. Meanwhile, the slip agents continue to migrate [3]. Whereby, the migration rate slows down with decreasing concentration [3]. So the stickiness phenomenon is believed to be dependent on the

- Duration of weathering of products,
- Photo-degradation rate of slip agents,
- Migration rate of slip agents to the surface, and
- Concentration of slip agents. [3]

Furthermore, the type of light stabilizer, such as hindered amine light stabilizer (HALS) usually used for TPOs, is indicated to have a strong influence on the phenomenon [3]. The low molecular mass light stabilizer migrates to the surface with the slip agents, where the HALS should decrease the photo-degradation rate of the polymer as well as the slip agents [3]. Therefore, the stickiness occurrence would be delayed [3]. On the other hand, if there are already degraded slip agent products, they would also be protected by the light stabilizers and extended stickiness on the surface [3]. In addition, the sticky touch of a surface is, generally, assessed by touching the parts' surface. This means significant dependencies on the human sense of touch, the human skin properties, and the environmental conditions during touching.

Adhesion – Adhesive joining

The assessment of stickiness by touching the surface can be described as a **weak adhesive connection** of two components like an adhesive joining. Therefore, the sticky layer on the surface is the adhesive and the human skin is the adherend. As herein before mentioned, it is suspected that slip agents are forming such a sticky layer.

However, the strength of an adhesive joint is determined by the system properties, such as the properties of the adhesive, the adherend, and the interphase [16]. The fundament mechanism, how one material adheres to another material, is not clearly identified [16]. There is no universally accepted relationship between specific atomic or molecular parameters at or near an interface and the strength of an adhesive bond [16]. To give a phenomenological understanding of mechanisms for the occurrence of adhesion the most widely accepted theories will be explained briefly: [16]

- **Mechanical interlocking** as a physically phenomenon influence the mechanical strength of many adhesive joints [16]. Surface roughening and some surface modification treatments are improving the mechanical interlocking or hooking [16].
- **Diffusion theory of adhesion** is based on the hypothesis that one material inerdiffuses into and with another [16]. It appears reasonable that a diffusion mechanism is involved in solvent bonding, commonly used to bond two pieces of materials like polymers [16].
- **Adsorption mechanisms** involve secondary molecular forces [16]. Molecules near the interface are believed to attract to each other by London dispersion forces, dipole-dipole interactions, hydrogen bonding, or other secondary molecular forces [16].
- **Chemical reaction theories** propose that chemical reactions occur between the adhesive and the adherend forming primary chemical bonds [16].
- **Electrostatic force model** of adhesion assumes that the electrons within the adhesive and the adherend occupy different energy levels and electron transfer occurs across the surface [16]. These opposite charges lead to an attraction [16].

2.3.1 State-of-the-art Experiments

There will be a brief experimental introduction about the most important attempts for assessing the stickiness phenomenon on polymer surfaces. These attempts are representing partly the state-of-the-art assessments – also measurements – of the automotive industry.

In the VW internal standard **PV 1306** [4] is defined a procedure for a laboratory stickiness assessment of PP-plastics. After an irradiation of the surfaces in an environmental chamber, such as described in Chapter 3.2, the specimens are assessed by touching of a tester in the hot state and classified according a list of eight levels. This classification is repeated five times for one specimen [4]. Thereby, one cycle is defined as a hot and dry weathering, where the specimen is faced to a Xenon arc light with following conditions: [4]

- Filter: Borosilicate/Soda lime
- Black standard temperature: (80±5) °C
- Specimen chamber temperature in the dry phase: (45±2) °C
- Relative humidity: (20±10) %
- Intensity of irradiation (300-400 nm): 40 W/m^2

These conditions are reported for the WeatherOmeter Ci4000 (Atlas Material Testing Technology GmbH; Linsengericht, GER) chamber and compared to the weathering conditions of the Kalahari-Test (see Chapter 3.2) milder. The duration of a cycle is defined as 96 h, which is equal to an irradiation dose of 96 MJ [4]. A disadvantage of this standard is that the assessment of stickness is subjective in terms of the need of well trained testers, which is required to be reproducible.

Another way to verify the stickiness on surfaces is to use the so-called **Sensotact (tactile) reference frame** [5]. In general, the function of this frame is based on comparing the specimen surfaces to a reference. Thereby, it is possible to define sense of stickiness, hardness, roughness, slippery etc. regarding specified movement procedures of the finger for each property [5]. All properties are classified with a reference surface and labeled with a number on the reverse side [5]. So, the tester is

possible to rank specimen surfaces according to this classification by touching [5]. The tactile reference frame is used in the automotive industry (e.g., Renault) as well as in other industries (e.g., toy manufacturing, textile industry etc.) [5]. Especially, for the stickiness references there are two disadvantages. First is that different colors were applied for some references, which could influence tester decisions. The second disadvantage is the observed differences in roughness, which in turn could affect assessing stickiness. Furthermore, it is still a subjective classification of stickiness. Thereby, it should be mentioned that there are also trainings offered [5].

The first attempt of an objective stickiness measurement methodology was published by Huber and Solera [2]. This so-called **Tack Test** is a test based on the ASTM D 3354 [17]. In this investigation the specimens were exposed both to Xenon arc light and to oven [2]. The UV exposure was carried out according to the SAE J 1885 protocol [18]. After exposure, a polyethylene low density (PE-LD) film was placed on each plaque completely covering the surface, while the specimens were still hot [2]. Specimen-film composites were then stacked together, where Teflon spacer was applied to separate them [2]. Then a weight (5 kg) was placed on the stack and left for 30 min to equilibrate at 89 °C [2]. Afterwards the specimen-film composites were tested with a Film Block Tester, where the force needed to separate the film was recorded as a measure for stickiness [2]. Unfortunately, in this investigation there is no report about the reproducibility of the test and the influence of the PE-LD film on the specimen's surface. Moreover, the test was limited by the maximum machine load of 2.1 N, but it was also reported that a value more than 0.2 N was very sticky.

2.4 Design of experiments

Since experiments involve the study of both the test parameter (factor) effects and the objects, which should be tested, it is important to get more information about the effects [19]. Factorial designs are a very efficient method for studying these effects [19]. Thereby, a factorial design is defined as the investigation of all possible combinations of the levels of the factors (treatment combinations) in each replication [19]. Furthermore, the effect of a factor is defined as the change in response (e.g., result

of the test) produced by a change in the level of the factor [19]. So, the factorial designs allow the effects of a factor to be estimated at several levels of the other factors, yielding conclusions that are valid over a range of experimental conditions [19].

2^3 factorial design

If three factors, each at two levels, are of interest, eight treatment combinations are necessary to evaluate the full factorial design statistically [19]. In Table 2.1 is the geometric notation ("+" high level, "-" low level) for the three factors (A, B, C), the interactions (AB, AC, BC, ABC), which is a multiplicative combination of the factors, and the notation for the treatment combinations illustrated [19].

Furthermore, the treatment combinations of a 2^3 factorial design can be illustrated graphically as a cube, where each corner of the cube represents a treatment combination [19]. Figure 2.6 demonstrates the 2^3 design as a graphic [19].

Table 2.1: The general tabulation of the treatment combinations' geometric notation of the eight runs (tests) for the 2^3 factorial design. Three factors (A, B, C); interactions (AB, AC, BC, ABC); "+" high level and "-" low level. **[19]**

Run	A	B	AB	C	AC	BC	ABC	Treatment Combination
1	-	-	+	-	+	+	-	(1)
2	+	-	-	-	-	+	+	a
3	-	+	-	-	+	-	+	b
4	+	+	+	-	-	-	-	ab
5	-	-	+	+	-	-	+	c
6	+	-	-	+	+	-	-	ac
7	-	+	-	+	-	+	-	bc
8	+	+	+	+	+	+	+	abc

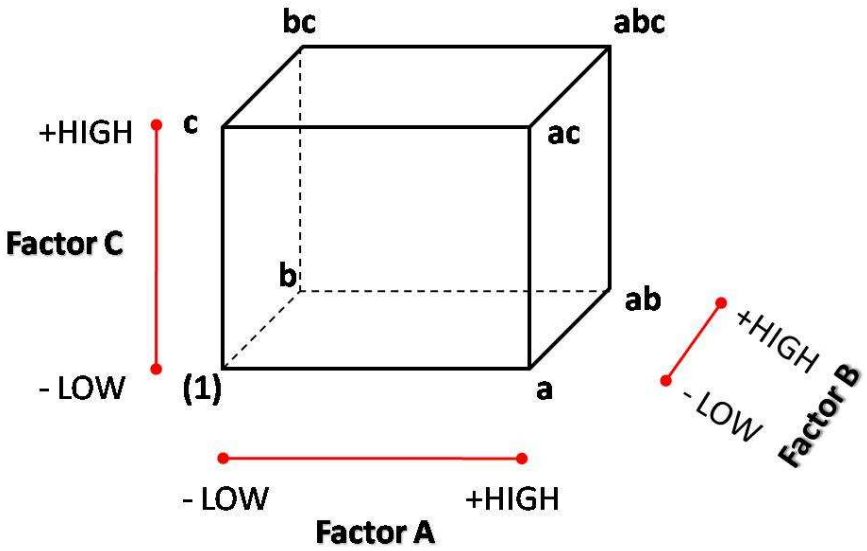

Figure 2.6: The graphically illustration of the 2^3 factorial design. **[19]**

The effect of a factor or interaction is the difference in averages between the four treatment combinations at high level minus the average of the four runs where the factor or interaction is at the low level [19]. Equation (1) and (2) show an example for a main effect and an interaction effect, respectively. Basically, the signs of the numerator of Equation (1) and (2) are determined according to Table 2.1. The *n* in the denominator of Equation (1) and (2) is the number of the treatment combinations' replicates (observations) [19]. Equation (1) can also be developed as a contrast (numerator) between the four treatment combinations in the right face of the cube (where A is at the high level) and the four in the left face (where A is at the low level) [19]. On the other hand, the Equation (2) can be developed as the difference in averages between runs on two diagonal planes in the cube, where the connection of abc, ab, c, (1) is one diagonal and the second diagonal is given by the connection of bc, b, ac, a (see Figure 2.6) [19].

$$A = \bar{y}_{A+} - \bar{y}_{A-} = \frac{a + ab + ac + abc}{4n} - \frac{(1) + b + c + bc}{4n} = \frac{1}{4n}[Contrast_A] \qquad (1)$$

$\bar{y}_{A+}$ … average of the observations, where factor A is at the high level
$\bar{y}_{A-}$ … average of the observations, where factor A is at the low level

$$AB = \bar{y}_{AB+} - \bar{y}_{AB-} = \frac{abc + ab + c + (1)}{4n} - \frac{bc + b + ac + a}{4n} = \frac{1}{4n}[Contrast_{AB}] \quad (2)$$

$\bar{y}_{AB+}$ … average of the observations, where factor A and B are at the high level
$\bar{y}_{AB-}$ … average of the observations, where factor A and B are at the low level

The test statistics (analysis of variance) for each main effect and interaction can be constructed by dividing the mean square for the effect or interaction by the mean square error, if all factors in the experiment are fixed, which means a specifically chosen number of levels for the factors A, B and C [19]. So, the interferences drawn from analysis of variance are valid only for the actual used levels [19]. Table 2.2 shows the analysis of variance table. Equation (3), (5) and (6) show the computation of the total sum of square, the sum of square of any effect and the error sum of square, respectively. Therefore, y_{ijkl} is the observed response when factor A is at the *i*th level (i = 1,2, … ,a), factor B is at the *j*th level (j = 1,2, … ,b) and factor C is at the *k*th level (k = 1,2, … ,c) for the *l*th replicate (l = 1,2 … ,n). The $y_{....}$ is the grand total of all the observations (see Equation (4)) [19].

$$SS_T = \sum_{i=1}^{a}\sum_{j=1}^{b}\sum_{k=1}^{c}\sum_{l=1}^{n} y_{ijkl}^2 - \frac{y_{....}^2}{abcn} \quad (3)$$

y_{ijkl} … observed response at the *i*th, *j*th and *k*th level for the *l*th replicate

$$y_{....} = \sum_{i=1}^{a}\sum_{j=1}^{b}\sum_{k=1}^{c}\sum_{l=1}^{n} y_{ijkl} \quad (4)$$

$$SS = \frac{Contrast^2}{8n} \quad (5)$$

$$SS_E = SS_T - SS_A - SS_B - \cdots - SS_{ABC} \quad (6)$$

Table 2.2: An Analysis of Variance (ANOVA) procedure for the 2^3 factorial design. **[19]**

Source of Variation	Sum of Squares	Degrees of Freedom (DoFr)	Mean Square	F_0
A	SS_A	a - 1	$MS_A = SS_A / DoFr$	$F_0 = MS_A / MS_E$
B	SS_B	b – 1	$MS_B = SS_B / DoFr$	$F_0 = MS_B / MS_E$
C	SS_C	c – 1	$MS_C = SS_C / DoFr$	$F_0 = MS_C / MS_E$
AB	SS_{AB}	(a - 1)(b - 1)	$MS_{AB} = SS_{AB} / DoFr$	$F_0 = MS_{AB} / MS_E$
AC	SS_{AC}	(a - 1)(c - 1)	$MS_{AC} = SS_{AC} / DoFr$	$F_0 = MS_{AC} / MS_E$
BC	SS_{BC}	(b - 1)(c - 1)	$MS_{BC} = SS_{BC} / DoFr$	$F_0 = MS_{BC} / MS_E$
ABC	SS_{ABC}	(a - 1)(b - 1)(c - 1)	$MS_{ABC} = SS_{ABC} / DoFr$	$F_0 = MS_{ABC} / MS_E$
Error	SS_E	abc(n - 1)	$MS_E = SS_E / DoFr$	
Total	SS_T	abcn - 1		

$$F_0 > F_{\alpha,(DoFr),abc(n-1)} \tag{7}$$

The F tests is performed, where the trueness of the null hypothesis H_0 (factor has no significance on the experiment) or the alternative hypothesis H_1 (factor has a significance) is verified [19]. H_0 will be rejected, if the constraint in Equation (7) is satisfied [19]. $F_{\alpha, (DoFr), abc(n-1)}$ is the upper-tail, one-tail critical value, which is tabled in any statistical book and F_0 is the calculated test (statistic) value (see Table 2.2) [19].

3 EXPERIMENTAL

In this section are the investigated materials, the specimens and the realized experiments described. Thereby, it will be focused on verifying the measured properties of the surfaces, and comparing these among each other. Furthermore, it will be partly described a statistical way to check the results relating to reliability.

3.1 Materials and Specimen

For the scratch and stickiness characterization of the model materials injection molded multigrain plaques were utilized. The multigrain plaques were produced according to VW standardized grains by BOREALIS Polyolefine Linz GmbH. To characterize the scratch and stickiness behavior of the materials the grain K09 and K29 were used, respectively. The geometry is defined by Eschmann Texture [20] (Texture Guide, Eschmann Textures International GmbH; Gummersbach, GER). The K09 and K29 surfaces are defined as grains with a grain depth of 0.12 mm and 0.01 mm, and a minimum draft angle of 6° and 1° for ejection from the injection molding tool, respectively [20]. These grains were cut out of the plaque with a bench shear. Figure 3.1 demonstrates schematically the VW multigrain plaque with their dimensions. The reason for testing on different grains was given by the fact that scratch visibility values are predominately measured on K09 at BOREALIS Polyolefine Linz GmbH. So there is a reference database evident for further comparisons of the measured model materials. However, the stickiness measure was verified on a smooth surface, such as K29, to minimize the influencing surface grain factors on this value.

Figure 3.2 and Figure 3.3 demonstrate the topography of the K09 and K29 grain, respectively. These topographies were measured with the aid of the FRT confocal white light microscope (MicroProf, Fries Research & Technology GmbH; Bergisch Gladbach, GER) at PCCL GmbH.

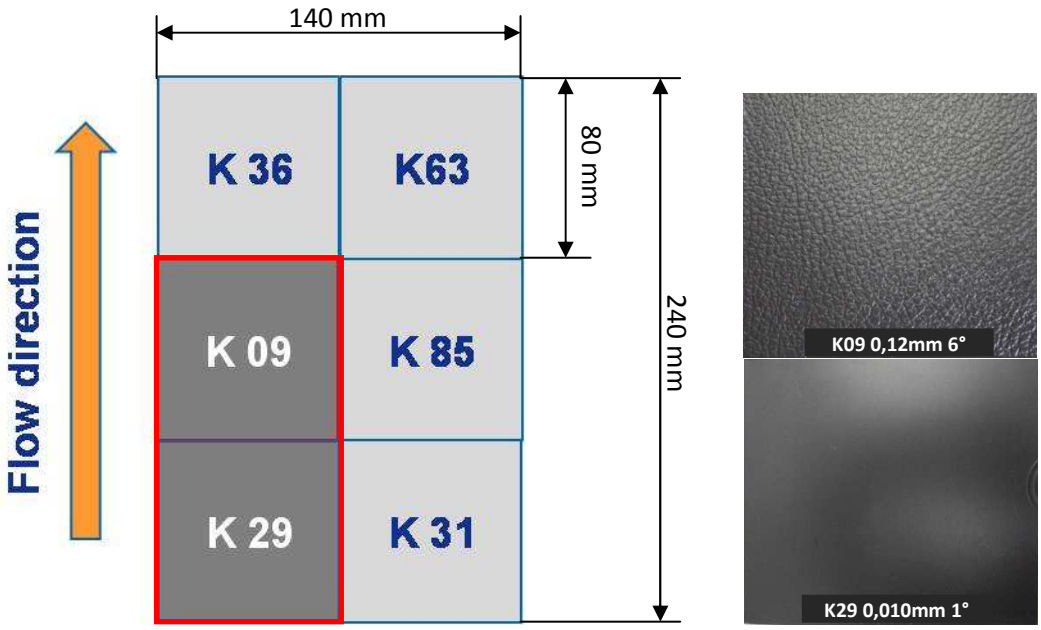

Figure 3.1: Schematically demonstration of the VW multigrain plaque and the cut of a specimen (K09 and K29). The thickness of the plaque is 3 mm.

Since the K09 grain is grosser compared to the K29 grain, a larger scan-area of (20x20) mm^2 was scanned for the K09 grain. The scan-area for K29 was (1x1) mm^2 in dimensions. From these topographies the arithmetic average roughness R_a were verified (see Figure 3.2 and Figure 3.3). The color of the topography's pixels demonstrates their height (the darker the color, the deeper the point).

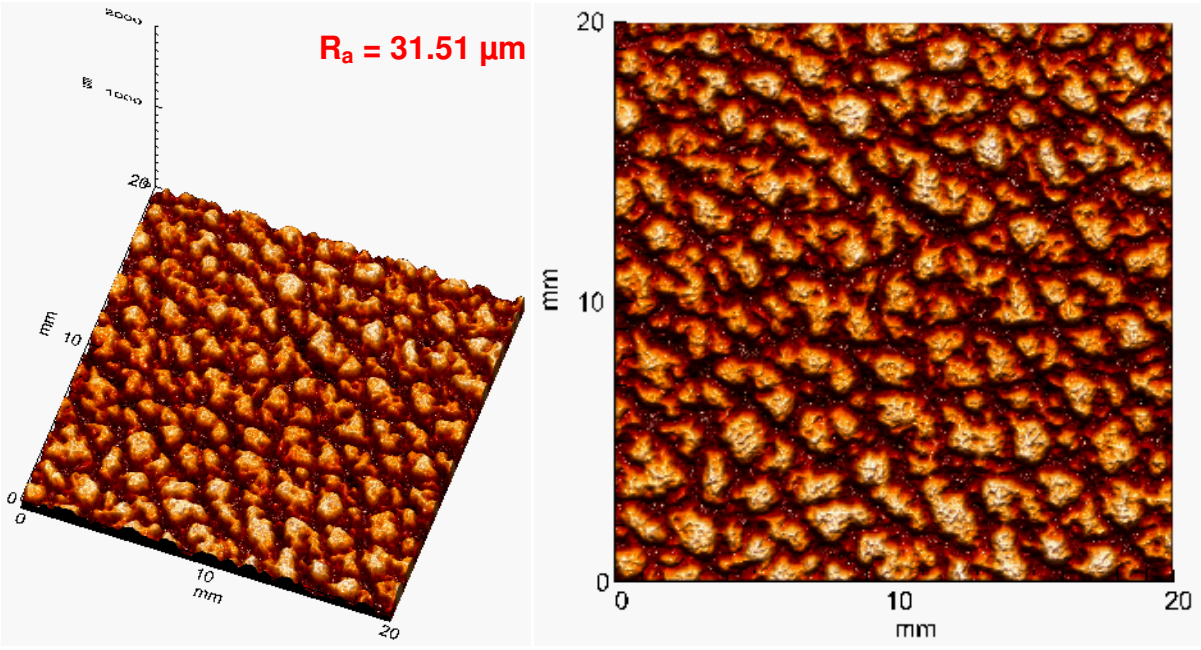

(a) **(b)**

Figure 3.2: Demonstration of the K09 grain's topography measured with the aid of the FRT confocal white light microscopy; **(a)** the 3D topography of K09, **(b)** the 2D topography of K09, scan-area = (20x20) mm^2.

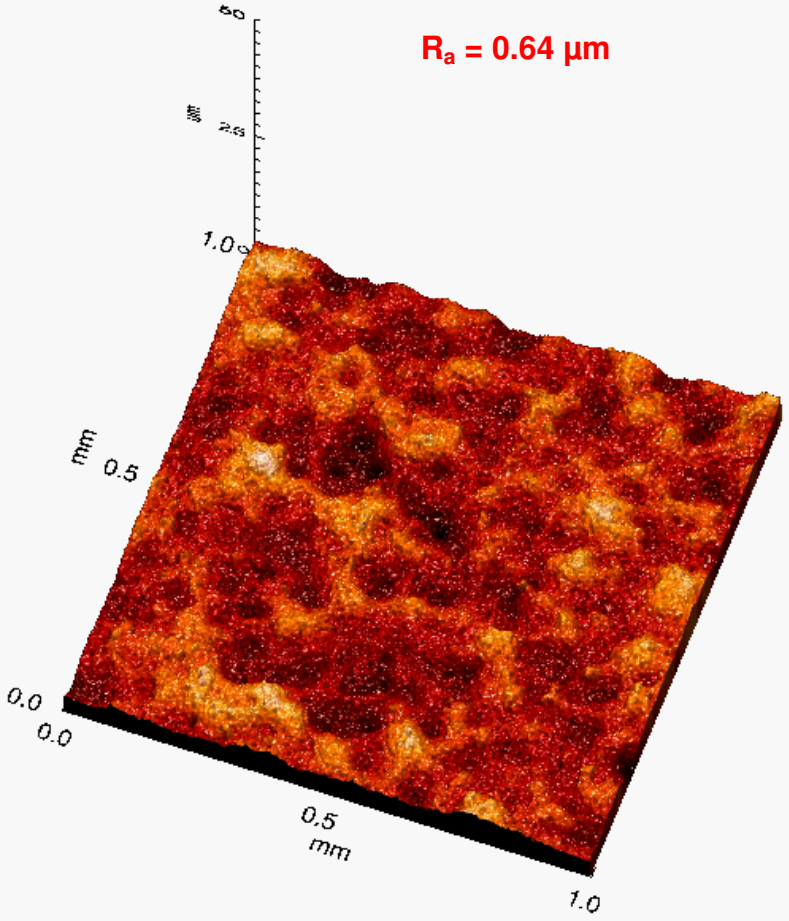

Figure 3.3: Demonstration of the K29 grain's topography measured with the aid of the FRT confocal white light microscopy; **(a)** the 3D topography of K09, **(b)** the 2D topography of K09, scan-area = (1x1) mm^2.

As previously described (see Chapter 2.3), the suspected reason for the occurrence of stickiness is the photo-degradation of surface lubricating slip additives. To verify this hypothesis, the TPO model materials were formulated with varying types of slip agent types. A schematically illustration of the TPO-compound-formulation is shown in Figure 3.4, where basically the constituents of base resin (RTPO), polyethylene high density (PE-HD), talc filler, antioxidants and UV-stabilizers were constant for all materials and only the slip agent is varied as both type and concentration. The addition of PE-HD gives beneficial advantage in stress whitening behavior and stabilizes the elastomeric phase of the TPO, while surface appearance relatively becomes worse. One of the antioxidants and UV-stabilizers, which were used for the model materials, were Irganox 1010 [21] and Chimassorb 119 [21], respectively. Moreover, the UV-stabilizer Cyasorb 2908 [22] was incorporated. Additional a black color masterbatch was used to provide appropriate visible contrast for measuring scratch visi-

bility. In the illustrated pie chart, the sectors are proportional to the concentration (wt%) of the represented constituent. Generally, this formulation is similar to a commercial automotive interior grade relating to the constant mass constituents.

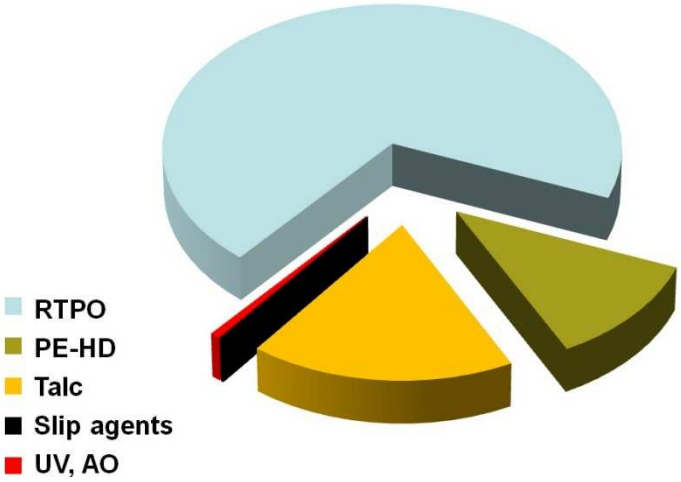

Figure 3.4: Schematically illustration of the TPO-formulation. The arc length of the sectors is equal to the concentration of the represented constituent.

The model TPO-compounds covered a serial of twelve materials (see Table 3.1). One material was composed of only the herein before mentioned constant constituents, without an incorporation of slip agents. Material 2 to 5 were incorporated with migratory slip agents. Their counterparts – nonmigratory slip agents – were represented by the formulation of materials 11 and 12. Moreover, there were also materials (6-10) with mixed slip agents formulated. Whereby, material 9 and 10 were incorporated with ready-made slip additive compounds. The exact components of these additives were not evident.

Table 3.1: Mass percentage (wt%) of the varied slip agents to enhance scratch resistance of the model TPO materials.

			N		OleA		EbS						SilA	
	Scratch Additives	unit	1	2	3	4	5	6	7	8	9	10	11	12
migratory	Erucamide	wt%		0.20				0.10						
	Oleamide	wt%			0.15				0.08					
	Stearamide	wt%				0.60								
	Ethylene-bis-Stearamide	wt%					0.60	0.10	0.08					
	Additive compound S	wt%								0.60	1.00			
	Additive compound SL	wt%										1.00		
non-mig	Silicone A	wt%											2.00	
	Silicone M	wt%												2.00

All material surfaces were scratch and stickiness characterized both unconditioned and conditioned. Here the term “conditioned” means after different durations of artificial weathering of the materials. Despite that, for the detailed interpretation of the results there will be only four materials discussed in detail. The neat, oleamide, ethylene-bis-stearamide, and silicone A were selected and named as N, OleA, EbS, and SilA, respectively. This materials represent the two main categorize of slip agents (migratory and nonmigratory). The two migratory slip agents differ from their molecular mass and saturation. Oleamide is an unsaturated and ethylene-bis-stearamide is a saturated fatty amide.

3.2 Artificial weathering

The Specimens were faced around a light source in an environmental chamber (WeatherOmeter Ci4000, Atlas Material Testing Technology GmbH; Linsengericht, GER) and so artificial weathered according to VW internal standard PV 3929 [23]. This standard, which is also known as Kalahari-Test, defines the weathering conditions in dry and hot climate for non-metallic materials [23]. It describes also the procedure for testing the aging behavior (e.g., change in color and gloss) of non-metallic materials. The weathering conditions of the chamber are: [23]

- Light source: Xenon arc light
- Filter: Pyres S
- Black standard temperature: (90±2) °C
- Specimen chamber temperature in the dry phase: (50±2) °C
- Relative humidity: (20±10) %
- Intensity of irradiation (300-400 nm): 75 W/m^2

In the current investigation the specimens were irradiated for **24 h**, **48 h**, **96 h**, **192 h**, and **384 h**. After irradiation the specimens were cooled for approximately 1 h and tested at room temperature. The tested characteristics included the change of color and gloss according to PV 3929, scratch visibility, and stickiness measurement.

3.3 Scratch visibility measurement

It should be mentioned that there are a large number of test methods to characterize scratch behavior. A few are standardized like ASTM D 7027 – 05 [12], others are internal standards of companies and numerous attempts to develop a test method are published. Nevertheless, there is no satisfactoring uniform method established now [11]. Unfortunately, the different test methods can normally not be compared with each other [11]. This situation affects the business between material suppliers such as BOREALIS Polyolefine Linz GmbH and OEMs. Many companies have their own well-proven methods to characterize scratch behavior of materials [11]. To fulfill the required quality, material suppliers must perform different methods for each company [11].

In the current study the Erichsen Test (Scratch Hardness Tester 430 P-I, Erichsen GmbH & Co.KG; Hemer, GER) was performed according to VW internal standard PV 3952 [24]. In this test the change in lightness ΔL^* is considered as a measure for scratch whitening/visibility (see Chapter 2.2.1). Figure 3.5 shows pictures of the Erichsen Tester during scratching. Basically, PV 3952 is a standard for testing scratch resistance of plastic-interior-parts. It covers coated as well as uncoated plastics for such application. The following procedure is defined to verify the scratch visibility: [24]

- Colorimetric evaluation with a spectrophotometric method, as defined in DIN 5033-4 [25], of color coordinates (L*, a*, b*) on unscratched surfaces with the use of the standard illuminant D65/10° according to DIN 6174 [26]; It is to average over minimum five evaluations;
- Scratching of a grid (40x40 mm) with 2 mm line spacing at room temperature (23±5) °C; defined dead-load and scratch-speed are 10 N and 1000 mm/min, respectively; The Erichsen scratch tester is to use with a stylus-tip-ball of Ø1 mm (Hardness Test Pencil Model 318, Erichsen GmbH & Co.KG; Hemer, D);
- Repeating of the colorimetric evaluation; change of the color coordinates (ΔL^*, Δa^*, Δb^*) is the measure for scratch visibility;

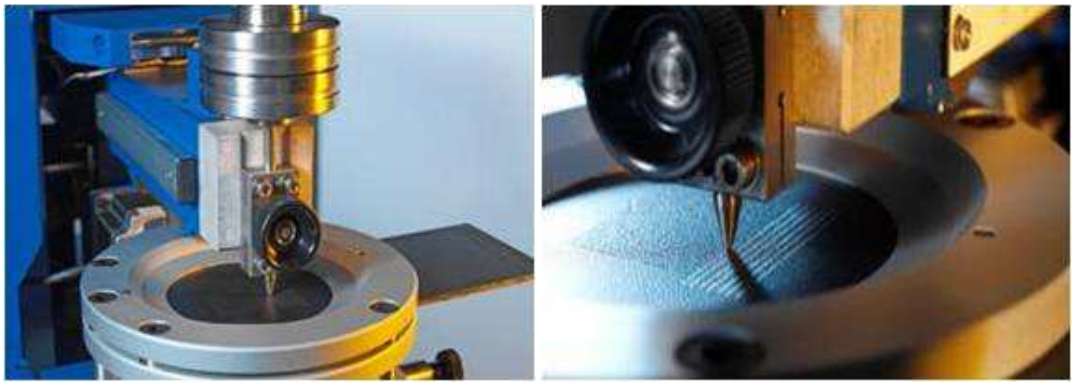

Figure 3.5: Pictures of the Erichsen Scratch Hardness Tester 430 P-I during scratching of a VW multigrain plaque.

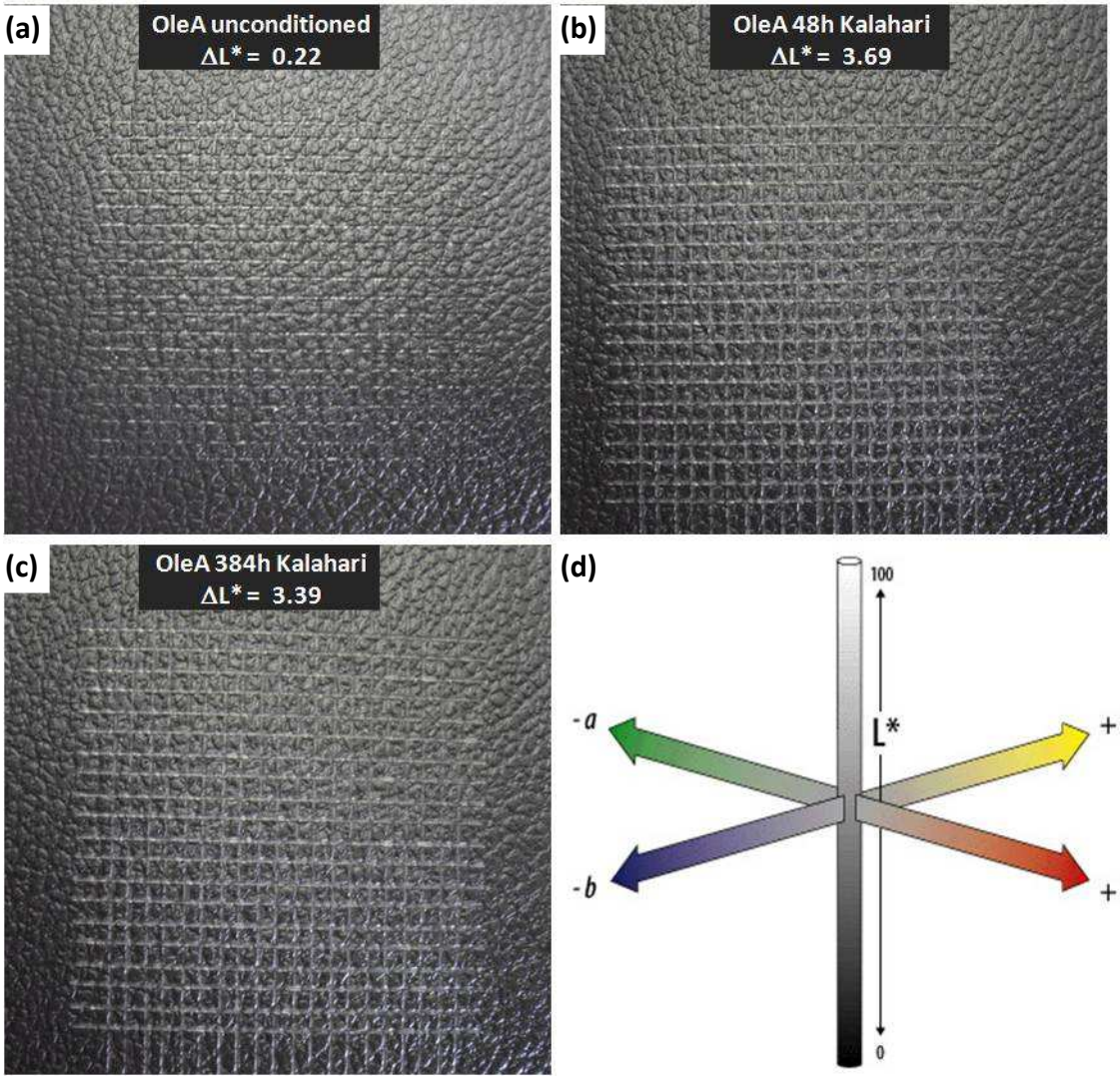

Figure 3.6: Demonstration of the scratch visibility results and pictures for both the unconditioned material OleA **(a)**, and after 48 h **(b)** and 384 h **(c)** Kalahari artificial weathering. Picture **(d)** illustrated the color coordinates (L*, a*, b*) **[27]**.

Figure 3.6 shows as examples of the scratched specimens of a model material OleA, where the anti-scratch additive oleamide has been incorporated. Since the investigated materials were black, only the change in lightness was the measure for the scratch visibility. Beginning from the unconditioned (a) to the Kalahari artificial weathered scratched specimens (b and c) clear changes in scratch visibility are observable. Here only two of five weathering durations are illustrated (48 h and 384 h Kalahari weathering). Furthermore, in Figure 3.6 (d) the axis of color coordinates (CIE Lab color-space) is illustrated, where **a** represents green and red, **b** blue and yellow, and **L** the lightness.

3.4 Stickiness measurement

Basically, the way from the requirements and the idea of a stickiness test to the finally defined procedure of measuring stickiness is described here. The first section will show the basic test parameters. In the second section the defined procedure and test parameters of the stickiness test are presented.

3.4.1 Development of a test methodology to characterize stickiness

Driven by the question: “How to measure the degree of stickiness?” the requirements for an ideal measurement were summarized as follows:

- Objective in terms of measured values instead of human impression
- Reproducible and reliable results
- Correlation with human sense of touch
- Easy to implement
- Enable short measurement times
- Flexible in terms of pretreatment (customer specifications)

The basic idea was to realize a compression-tensile test combination, where a die was first vertically pressed on the surface with a constant controlled force. After a holding time, the die was detracted displacement controlled (constant haul-off speed). The force (stickiness force), which was necessary to remove the die vertical-

ly, was a measure for the stickiness. In general, this procedure of verifying stickiness is similar to the manual assessing by touching without a horizontal movement of the finger like the Sensotact [5] stickiness assessing. However, the test parameters had to be verified regarding their significance and influence on measured stickiness force. The variable test parameters were the compressive force, the hold-time at compressive force of the die on the specimen's surface, the haul-off speed and the material of the die tip.

First of all, the material of the die tip had to be chosen for the further verification of the parameter influences. A soft, easy to machine and long-term available material was desired. The material of choice was an elastomer, which does not contain migrating constituents and does not have a sticky surface. It was observed, that a natural rubber/styrene butadiene rubber (NR/SBR) blend (Semperflex A 560, Semperit Technische Produkte GmbH; Wimpassing, A) gave the optimal balance between hardness and low sticky surface. In Table 3.2 is the material's behavior of the Semperflex A 560 tabulated. Additionally, the surface topography was measured with the use of a confocal laser scanning microscopy at BOREALIS Polyolefine Linz GmbH to verify the arithmetic average roughness R_a of both sides of the elastomer sheet.

Since the die tip elastomer alters the mechanical properties during the life time (see aging behavior in Table 3.2), the die tip will not show the same behavior after long time and/or high temperature during stickiness testing. However, the testing time of the stickiness quotient is very short and for each reference-specimen combination a new elastomer is used. So, the elastomer's properties are assumed to be constant for this short testing time-window (see Figure 3.7).

Table 3.2: The material's behavior of the die tip material Semperflex A 560 are listed according to **[28]**. In addition, the measured R_a (confocal laser scanning microscope) is tabulated for both sides of the elastomer sides.

Mechanical Properties	
Hardness [Shore A]:	40 ±5
Density [g/cm^3]:	1.06
Tensile strength [N/mm^2]:	18
Elongation at break [%]:	600
Chemical Resistance	
Ozone resistance:	non resistant
Weather resistance:	non resistant
Oil resistance:	non resistant
Benzine resistance:	non resistant
Acid resistance:	moderately resistant
Strong bases:	resistant
Abrasion resistance:	good suitable
Aging DIN 53508	
Conditions:	70 h / 70 °C
Hardness:	+3 Shore A
Strength:	-10%
Elongation:	-15%
R_a [µm] / CLSM	
Side 1:	1.17
Side 2:	1.84

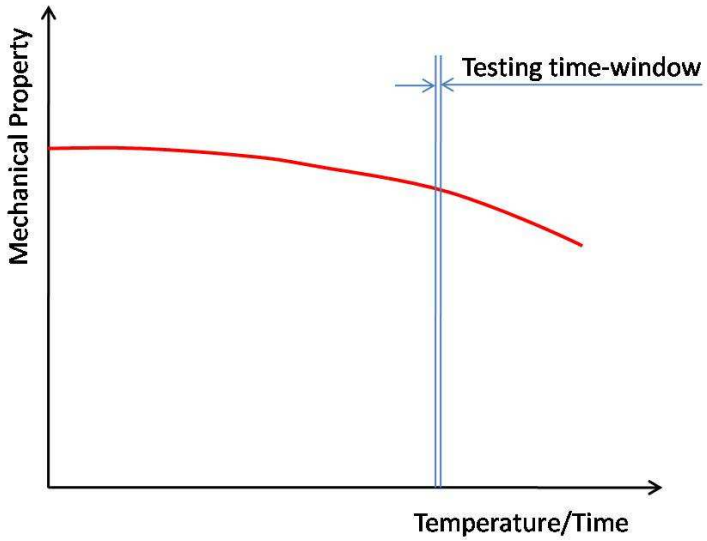

Figure 3.7: Schematic illustration of the time and temperature dependent change of the die tip elastomer mechanical properties (aging) and the very short testing time-window, where the elastomer has during the stickiness test constant material behavior.

To verify the influences of the parameters compressive force, hold-time and haul-off speed a design of experiments was applied, where for each factor two levels were defined. A three factors and two levels (2^3) design of experiments, which requires eight experiments to analyze the significance of each factor, was performed (see Table 3.3 and Chapter 2.4).

Table 3.3: Listing of performed test with different level of the factors according to 2^3 design of experiments; yellow ➔ low level, orange ➔ high level.

Test#	F	t_H	v	Treatment Combination
/	N	s	mm/s	/
1	-5	1	10	**(1)**
10	-5	1	100	**c**
5	-5	180	10	**b**
7	-5	180	100	**bc**
8	-50	1	10	**a**
6	-50	1	100	**ac**
4	-50	180	10	**ab**
2	-50	180	100	**abc**

Then the results were analyzed according to the statistical procedures of analysis of variance (ANOVA) including an F test to see, if the factors were significant for the response value – stickiness – or not (see Table 2.2). Thereby, the response quantity of the test method for the degree of stickiness was defined as the quotient of specimens' and references' stickiness forces (see Equation (8)).

$$StickinessQuotient = \frac{StickinessForce\ Specimen}{StickinessForce\ Reference} \tag{8}$$

An aluminum sheet was chosen as reference for the measurement caused by their easy to clean and almost unchangeable surface properties. The reason for a reference was to minimize the inherent fluctuation of an engineering material, such as the die tip elastomer, and so to increase the reproducibility of the test. Moreover, to reduce the possibility of transferring surface components from one specimen to another a new elastomer was used for each specimen characterization. In addition, every elastomer was cleaned with acetone before measuring to remove contaminations. A

detailed explanation of the applied cleaning condition will be discussed in Chapter 4.1.1.

3.4.2 Stickiness *Test*

Basically, this test methodology can be adopted for every tensile testing machine, where the possibility is given to set-up the test parameters. Figure 3.8 shows pictures of the set-up both schematically and during measuring the aluminum reference. For the current investigations an Instron tensile testing machine (ElectroPuls E3000, Instron Deutschland GmbH; Darmstadt, GER) was used to perform the experiments.

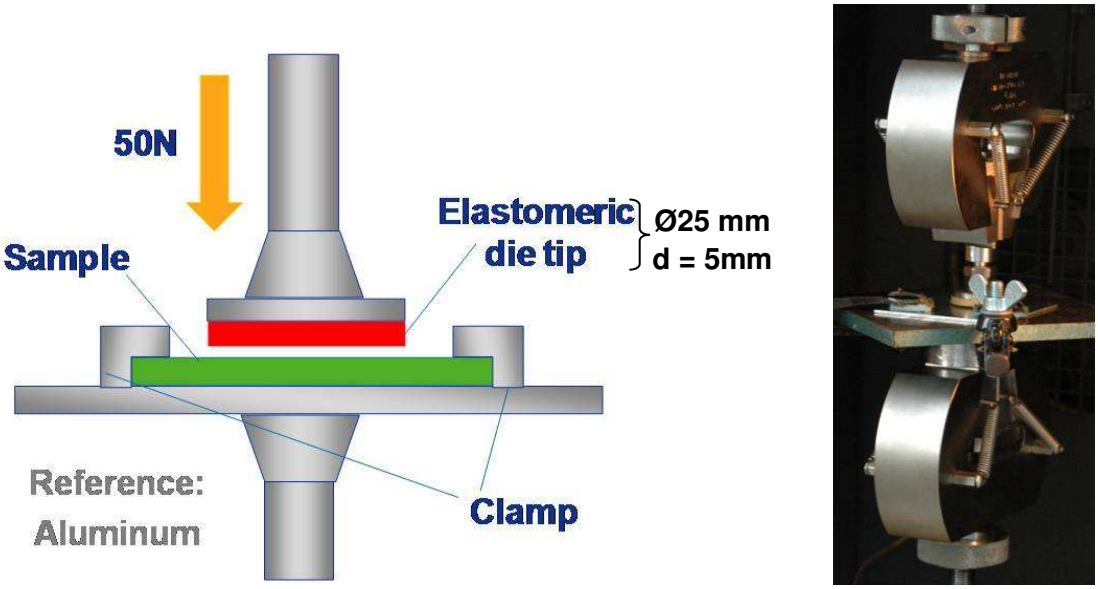

Figure 3.8: Pictures of the developed methodology (stickiness test).

The defined procedure of the stickiness test comprises the following steps:

- Clean die tip elastomer (NR/SBR),
- Use double-side adhesive tape to attach the elastomer tip on the die,
- Measure stickiness force on aluminum reference and calculate average over three tests,
- Measure stickiness force on specimen and calculate average over three tests, and
- Finally calculate stickiness quotient;

The defined optimal test parameters are:

- Compressive force, F = -50 N,
- Hold-time, t_H = 91 s,
- Haul-off speed, v = 55 mm/s;

Figure 3.9 and Figure 3.10 show the stickiness measurement process of the stickiness test in the force-displacement and in the displacement-time graphs of the die tip elastomer, respectively.

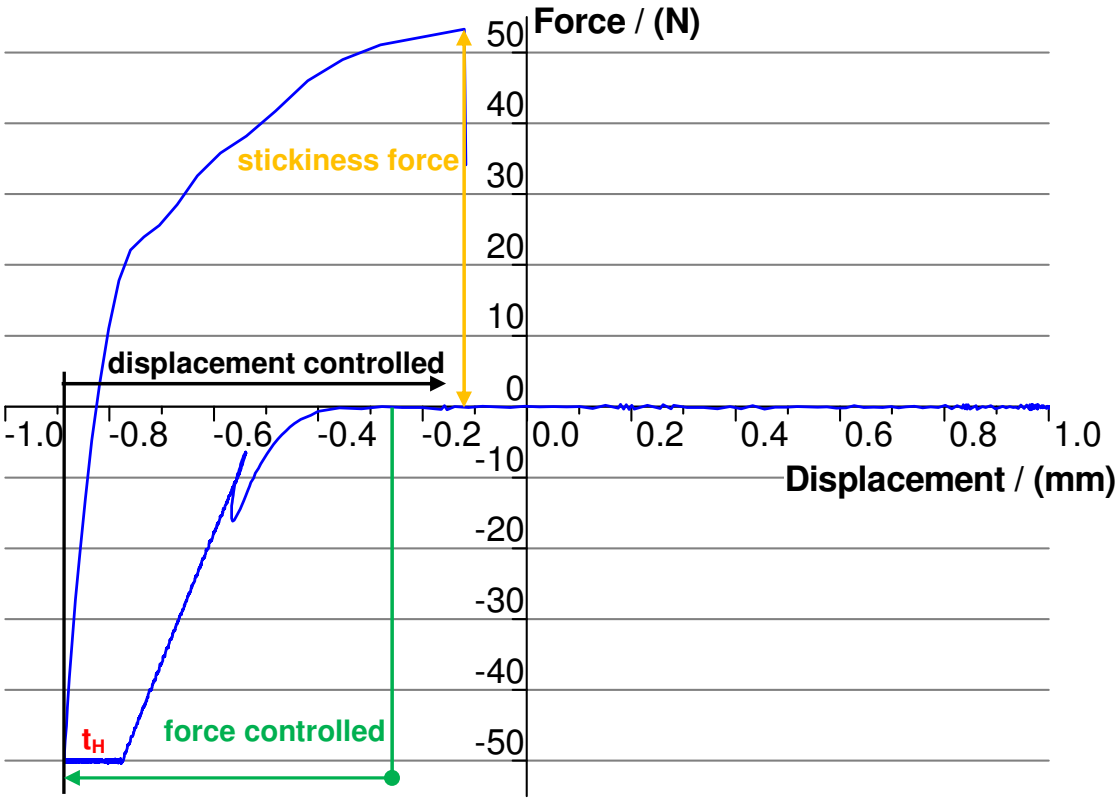

Figure 3.9: Demonstration of the stickiness test's measurement process in the force-displacement graph of the die tip elastomer. Material: aluminum (reference)

In the force-displacement graph (see Figure 3.9) the two phases of the stickiness test and the stickiness force evaluation are illustrated. The first phase is force controlled at -50 N until the hold-time (91 s) runs off. During this phase the die tip elastomer is creeping at constant force (see Figure 3.10). After approximately 40 s, the displacement is almost at a constant value. In the second phase, which is displacement controlled (55 mm/s), the peak value in the force-displacement curve was reported as stickiness force, i.e. force needed to remove the die tip from the specimen's surface.

When the die is removed from the surface, the oscillation of the die is measured (see Figure 3.9).

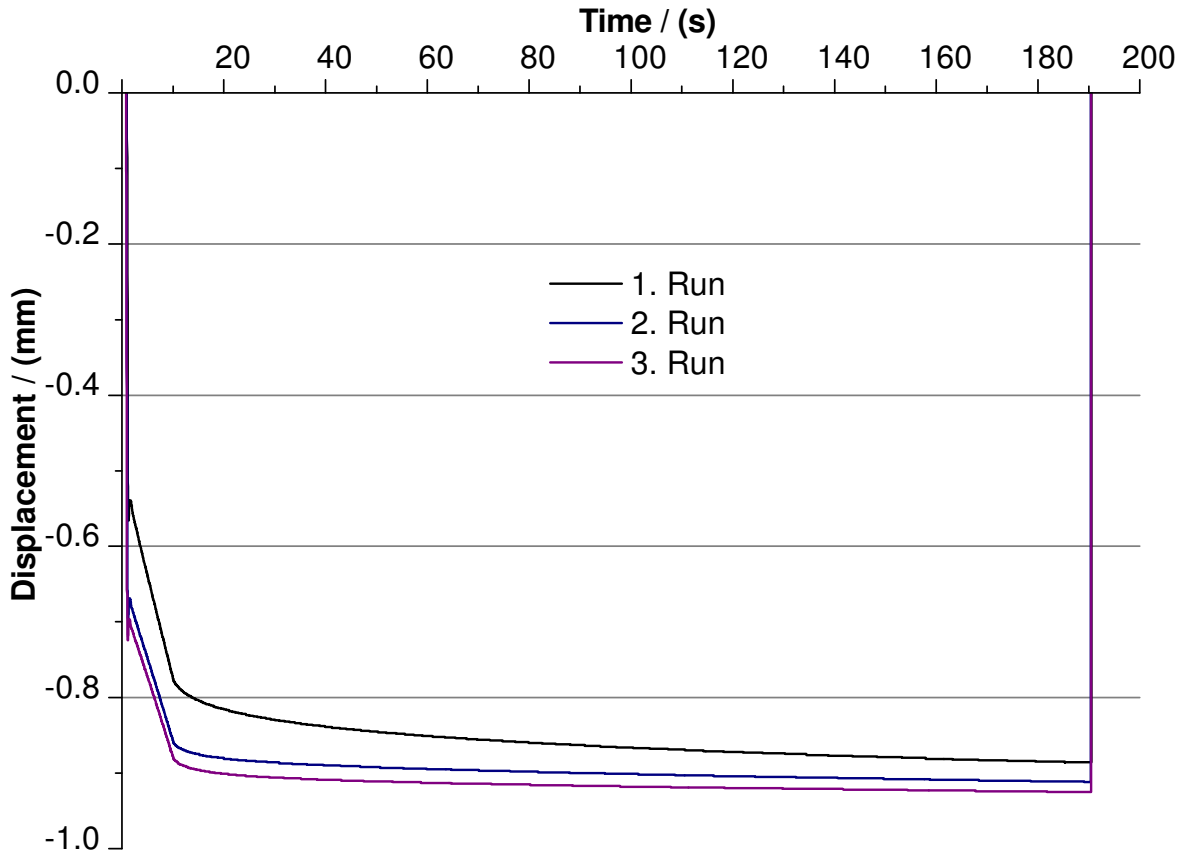

Figure 3.10: The displacement-time graph of the stickiness test's measurement process for three test runs are illustrated. Here the creep of the die tip elastomer is visible. Material: aluminum (reference)

According to this testing condition all materials were characterized at room temperature, also the weathered specimens (approximately 1 h cooling). To verify if the test is correlating with the human sense of touch a haptic panel was organized (see Chapter 3.5).

3.5 Haptic panel

The objective of this panel was to verify, if the stickiness methodology is correlating to the human sense of touch. Hence, employees of BOREALIS Polyolefine Linz GmbH were trained to assess and rank different sticky surfaces by touching according to Sensotact reference frame [5]. Then two haptic panel sessions were organized,

where the stickiness of four model materials was ranked from lowest to highest after 48 h Kalahari irradiation. These four materials were the highlighted materials in Table 3.1. The procedure of these panels was according to DIN 10963 [29], which is equivalent to ISO 8587:1988. Therefore, the panels were performed specially in a conditioned Sensory Laboratory at 23 °C and 50% relative humidity. Form each material four specimens were prepared and divided into four sections. These sections were labeled in alphabetical order. On the first session 16 tester and on the second 12 tester assessed the surfaces. Figure 3.11 shows a picture of a haptic panel session.

Figure 3.11: Picture of the Sensory Laboratory and specimens during a session of haptic panel.

The testers were instructed to following order:

- Wash your hands,
- Use **forefinger, middle finger** and **ring finger** for touching the samples at an angle of **approximately 15°**;
  The necessary force to remove the fingers vertically is a measure for stickiness.
- **Rank samples** with increasing stickiness; highest to lowest with 4 to 1, respectively;

Afterwards, the ranks were tabulated for a further statistical evaluation. However, the pH-value and the moisture of the testers' fingers are also influencing their sense of touch. This fact was not considered in the haptic panel. The testers were only instructed to wash their hands.

Statistical Interpretation: Friedman-Test

One of the most common statistical tests to evaluate rankings of dependent samplings is the Friedman-Test. The results of the test show relating to the ranking-property both if the *k* specimens are ranked significantly different by the *n* testers and if pairs of the *k* specimens are significantly different. Basically, the Friedman value *F* is calculated according to Equation (9) and compared to a critical value, which are tabulated in [29] regarding *n*, *k*, and level of significance *α*. If the calculated value is equal or greater than the critical value, there are significant differences within the specimens.

$$F = \frac{12}{n \cdot k \cdot (k+1)} \cdot (R_1^2 + R_2^2 + \cdots + R_k^2) - 3 \cdot n \cdot (k+1) \geq F_{crit} \quad (9)$$

n	Number of testers
k	Number of specimens
$R_1, R_2 \ldots R_k$	Sum of ranks

$$|R_A - R_B| \geq 1.960 \cdot \sqrt{\frac{n \cdot k \cdot (k+1)}{6}} \qquad (\alpha = 5\,\%) \quad (10)$$

$$|R_A - R_B| \geq 2.576 \cdot \sqrt{\frac{n \cdot k \cdot (k+1)}{6}} \qquad (\alpha = 1\,\%) \quad (11)$$

If there are general differences regarding Equation (9), the sum of ranks can be used to compare pairs of specimens. Hence, differences between pairs of specimens can be verified according to Equation (10) and (11) for a level of significance of 5% and 1%, respectively. If Equation (10) and/or (11) is not satisfied for the differences of the sum of ranks, the pairs are either significant for a lower level or not significant at all.

3.6 Fourier Transformed Infrared Spectroscopy

From the materials surfaces FT-IR spectra (Spectrum GX, PerkinElmer; Massachusetts, USA) were measured both in the unconditioned state and after 48 h weathering. The spectra were measured on the K29 grain of the multigrain plaques (see Fig-

ure 3.1). Thereby, it was expected to detect the presence of additives as well as degradation products (e.g., alcohols, ketons), which could be the reason for the sticky touch, on the TPO surfaces. The spectra of the neat anti-scratch additives, which have been used for the formulation of the investigated materials, are illustrated in the following from Figure 3.12 to Figure 3.14. There are also the characteristic bands highlighted, which indicate the migration of the additives. Furthermore, the spectra of an antioxidant (Irganox 1010) and an UV stabilizer (Chimassorb 119) are illustrated in Figure 3.15 and in Figure 3.16 respectively. Unfortunately, the spectrum of the neat additive Cyasorb 2908 (UV-stabilizer) was not available. However, the characteristic band for this additive is at approximately 1740 cm^{-1}.

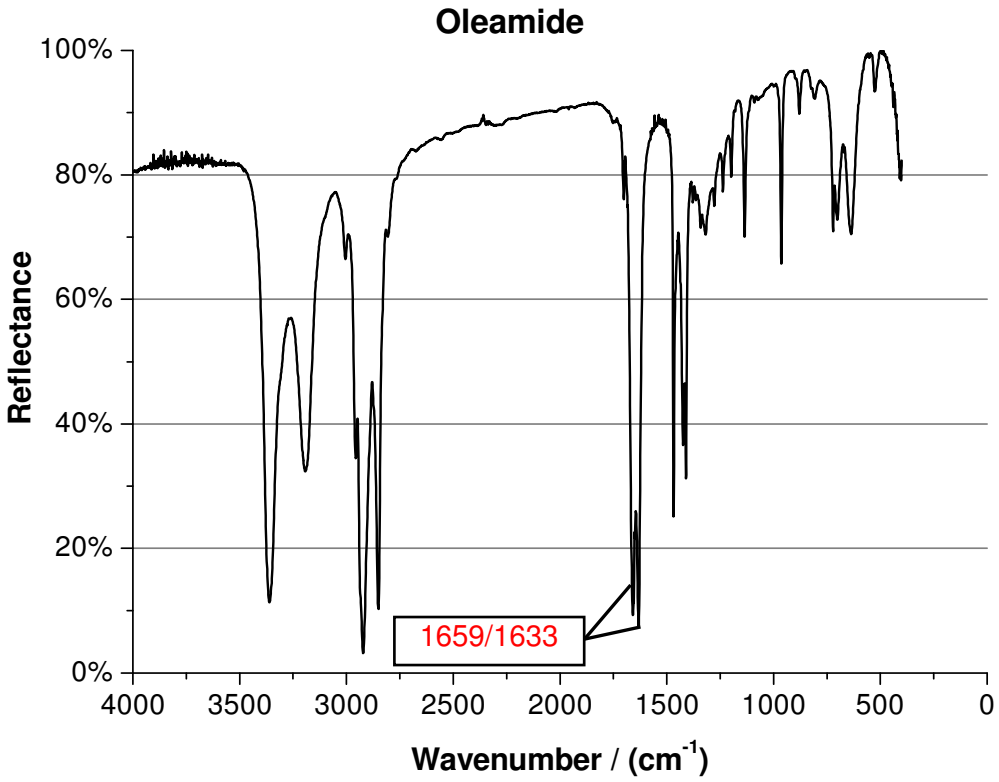

Figure 3.12: The spectrum of the anti-scratch additive oleamide, which was formulated into the material OleA.

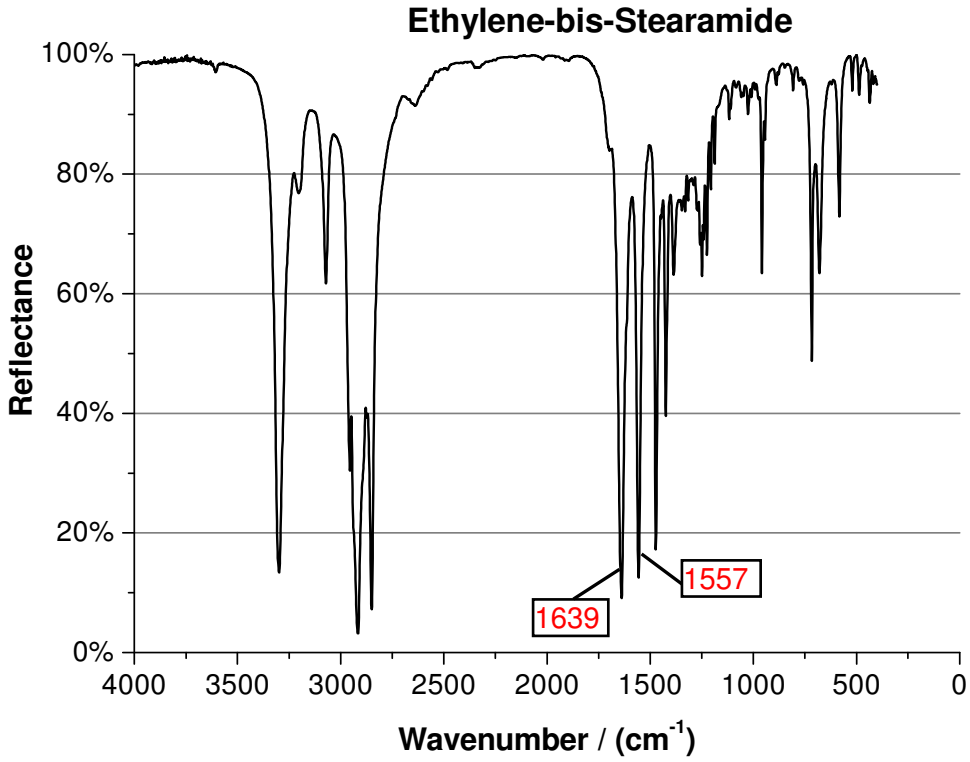

Figure 3.13: The spectrum of the anti-scratch additive ethylene-bis-stearamide, which was formulated into the material EbS.

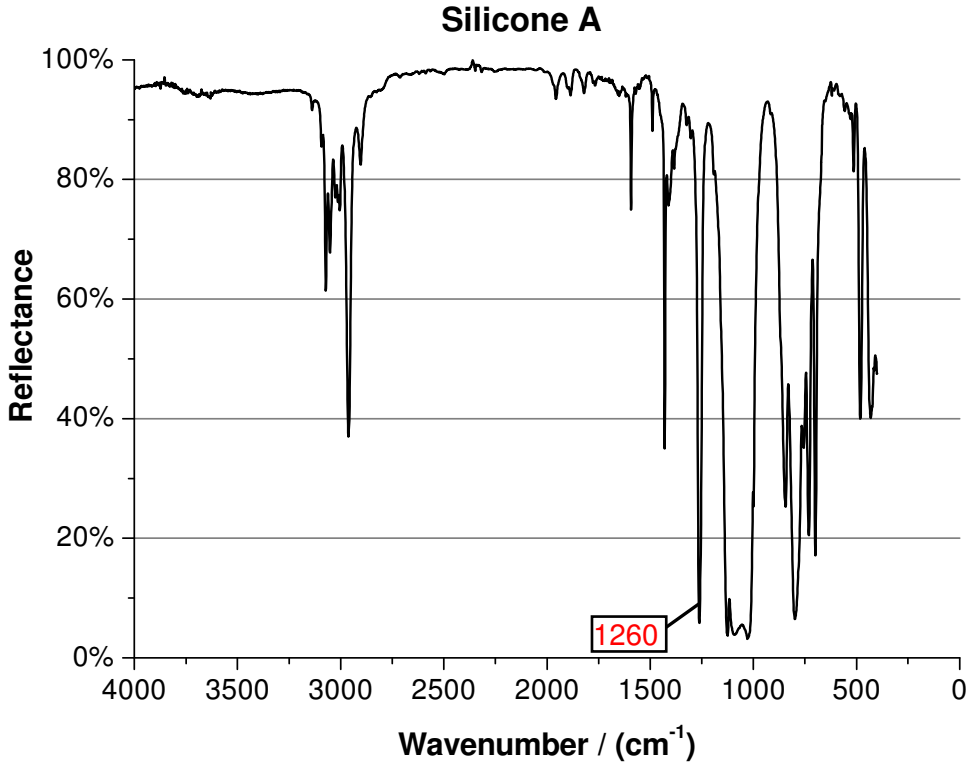

Figure 3.14: The spectrum of the anti-scratch additive silicone A, which was formulated into the material SilA.

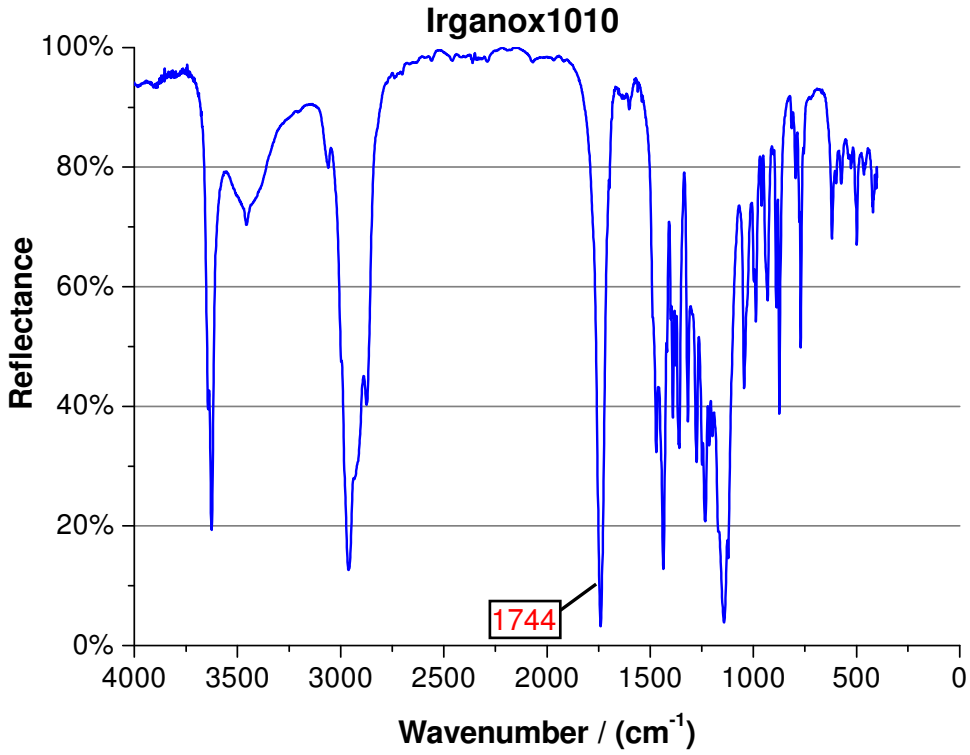

Figure 3.15: The spectrum of the antioxidant additive Irganox 1010, which was formulated into all materials.

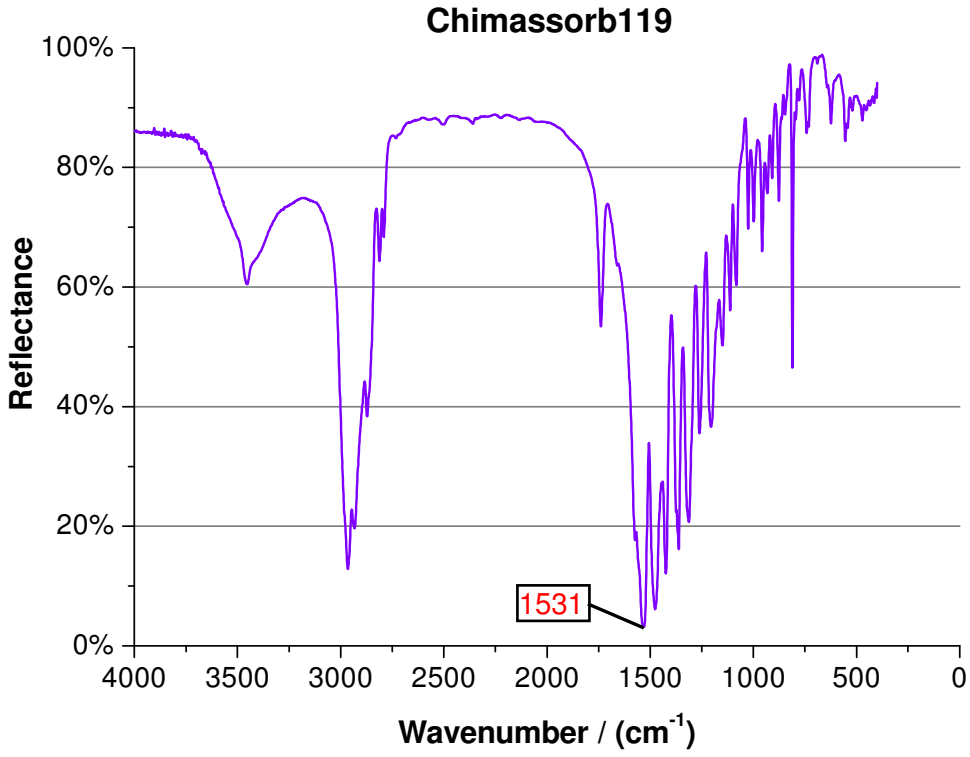

Figure 3.16: The spectrum of the UV stabilizer additive Chimassorb 119, which was formulated into all materials.

4 RESULTS AND DISCUSSION

The objective of this work was to characterize the scratch and stickiness behavior of several model PP-compounds and to find the material's formulation with the best surface performance solution for automotive interior applications. Before the illustration and discussion of the scratch visibility and stickiness quotient results, the results of the method development will be discussed. These results include also the demonstration of the haptic panel to examine, if the stickiness test is correlating to human assessing.

4.1 Preliminary evaluation of the stickiness test methodology

First of all, the results during the validation of the developed test methodology will be presented. This validation was necessary to ensure the reproducibility and reliability of the test. The main focuses included the verification of the best cleaning condition and the statistical evaluation and interpretation of the designed experiments to define the test parameters compressive force, hold-time at compressive force and haul-off speed.

4.1.1 Cleaning conditions

Due to handling reasons the elastomers (Semperflex A 560) was provided with a separating agent on its surface. So, the fluctuation of the stickiness test results was very high. Consequently, different cleaning conditions were tested to verify their benefit in terms of low standard deviation. Several test runs were performed for each cleaning condition of the elastomer and uncleaned elastomer. The cleaning condition included water and acetone cleaning. Thereby, the acetone cleaned elastomer die tips were tested both immediately after cleaning and after 24 h to verify if acetone leads to a time dependent change of the elastomer surface and further to a change of the test results. The test run was repeated three times and the average stickiness forces, the average stickiness quotient S/R and the standard deviation of both the specimen's stickiness forces and the reference's stickiness forces were evaluated. Therefore, the tests were measured according to the herein before listed procedure

in Chapter 3.4.2. But the test parameters were different in terms of the haul-off speed (100 mm/s instead of 55 mm/s for the optimal parameter). Since the validation of the cleaning conditions was performed before the actual design of the experiments, the here used parameters were predefined to focus on the cleaning conditions only.

Table 4.1 shows the results of the measured stickiness force and the calculated mean, mean stickiness quotient S/R and the standard deviation STDEV. Thereby, the column EA (orange) is representing the water cleaned elastomer die tip results, EB (green) the uncleaned, EC (blue) the acetone cleaned and ED (violet) the acetone cleaned and after 24 h measured.

Table 4.1: The stickiness force results to validate the influences of different cleaning conditions of the elastomer die tips. Of these results the mean, the mean stickiness quotient S/R and the standard deviation STDEV were calculated; E … elastomer, A, B, C, D … cleaning condition, 1, 2, 3 … numbering of the different elastomers, R … reference, S … specimen.

	water **EA-1**		*uncleaned* **EB-1**		*acetone* **EC-1**		*acetone&24h* **ED-1**	
	R (N)	**S** (N)	**R** (N)	**S** (N)	**R** (N)	**S** (N)	**R** (N)	**S** (N)
1	38,39	22,78	21,29	14,82	63,58	24,94	67,01	26,28
2	41,92	20,99	22,37	15,36	73,03	27,23	72,70	28,45
3	43,23	21,34	24,04	15,66	75,20	27,53	73,96	27,71
mean	*41,18*	*21,70*	*22,57*	*15,28*	*70,60*	*26,57*	*71,22*	*27,48*
S/R	**0,53**		**0,68**		**0,38**		**0,39**	
STDEV	2,50	0,95	1,39	0,43	6,18	1,42	3,70	1,10
	EA-2		**EB-2**		**EC-2**		**ED-2**	
	R (N)	**S** (N)	**R** (N)	**S** (N)	**R** (N)	**S** (N)	**R** (N)	**S** (N)
1	31,13	11,89	28,37	12,89	87,29	36,92	95,14	34,01
2	32,17	11,64	30,55	14,56	94,39	38,92	95,73	34,86
3	32,48	11,56	30,77	14,49	95,44	39,09	95,11	34,72
mean	*31,93*	*11,70*	*29,90*	*13,98*	*92,37*	*38,31*	*95,33*	*34,53*
S/R	**0,37**		**0,47**		**0,41**		**0,36**	
STDEV	0,71	0,17	1,33	0,94	4,43	1,21	0,35	0,46
	EA-3		**EB-3**		**EC-3**		**ED-3**	
	R (N)	**S** (N)	**R** (N)	**S** (N)	**R** (N)	**S** (N)	**R** (N)	**S** (N)
1	18,72	10,36	27,31	8,59	84,19	28,98	74,66	23,67
2	26,26	10,99	30,05	8,78	86,11	29,82	76,71	27,67
3	28,90	10,97	31,33	9,22	86,23	29,72	74,86	30,84
mean	*24,63*	*10,77*	*29,56*	*8,86*	*85,51*	*29,51*	*75,41*	*27,39*
S/R	**0,44**		**0,30**		**0,35**		**0,36**	
STDEV	5,28	0,36	2,05	0,32	1,14	0,46	1,13	3,59
STDEV of S/R	**0,08**		**0,19**		**0,03**		**0,01**	

The results of the standard deviation STDEV of S/R show the lowest value for the acetone cleaned elastomer die tips. The highest value is evident for the uncleaned elastomers. Since the effect of acetone on the elastomers' surface is short and the standard deviation of the stickiness quotient is low, the cleaning condition of choice is acetone cleaning. Furthermore, the results show a high reproducibility of the stickiness test. This is illustrated in Figure 4.1, where the measured stickiness forces and the standard deviations are shown for both the reference and the specimen. Each test run was measured with an acetone cleaned elastomer.

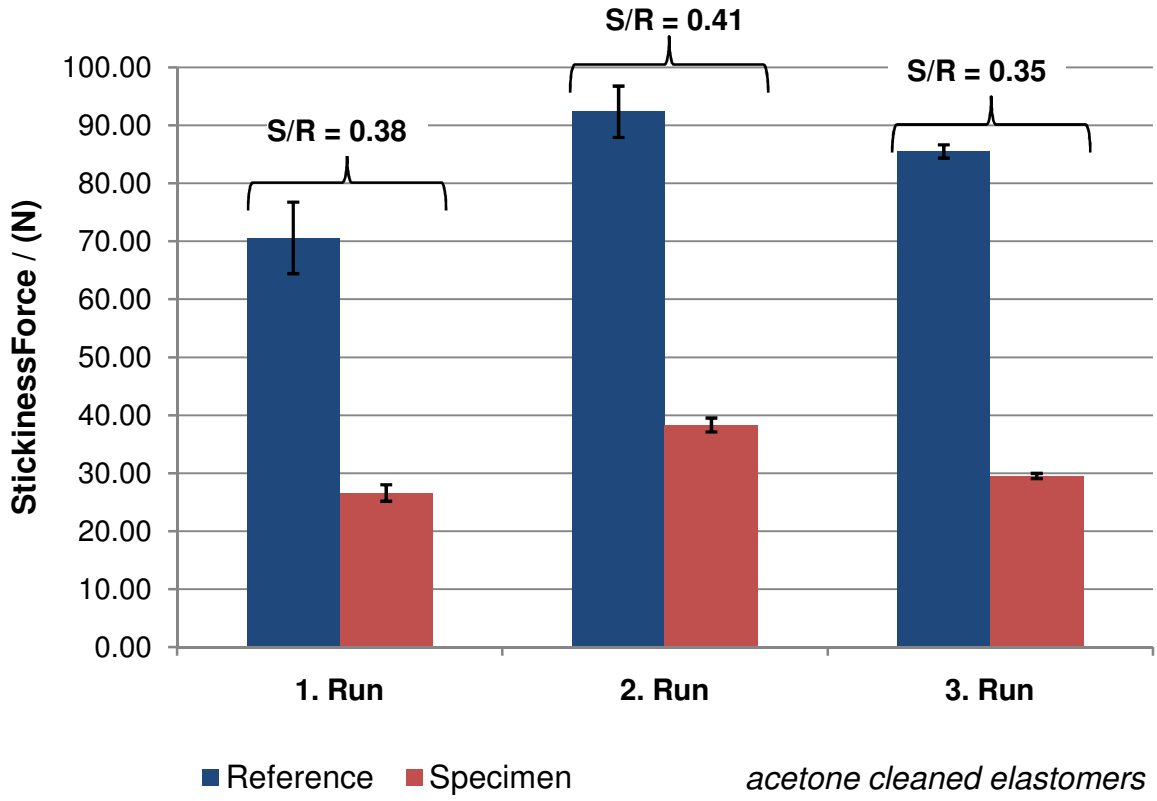

Figure 4.1: Demonstration of the measured stickiness forces (y-axis) and the standard deviations of the reference and the specimens. Reference and specimen were measured three times (1. run to 3. run). Also the stickiness quotients for each test run are illustrated.

4.1.2 Design of experiments results

After the definition of the die tip elastomer's cleaning condition, the other test parameters, which also influence the stickiness test, had to be standardized. Therefore,

the 2^3 factorial design was performed (see Chapter 2.4 and 3.4.1) with the material N (without anti-scratch additives), where these three test parameters (factors):

A ➔ Compressive force
B ➔ Hold-time at compressive force of the die tip on the specimen's surface
C ➔ Haul-off speed

were varied between two levels, to see how a change of a factor (main effect) or more factors (interaction effect) influence on the stickiness quotient (response value). The combinations of the systematically varying levels of test parameters are listed in Table 3.3. Table 4.2 shows the results of the designed experiments, where the treatment combination column indicates, which factors are at high level (e.g., **abc** ➔ all factors are at high level, **c** ➔ factor C is at high level and A, B are at low level, and **(1)** ➔ all factors are at low level). All treatment combinations were repeated three times and the mean stickiness quotient S/R and the sum of the results $y_{ijk.}$ were computed. The tests were carried out randomized according to the test number to avoid systematical errors by changing only one parameter from a treatment combination to another. From these results it is visible that a change of the Factors B and C (hold-time and haul-off speed) does not affect the stickiness quotient very much (compare treatment combination **c**, **b**, **bc** and **(1)**, but also **a** vs. **ac**, **a** vs. **ab** etc.). On the other hand, the influence of factor A (compressive force) is very high (see treatment combination **bc** vs. **abc**, **(1)** vs. **a**, **c** vs. **ac** and **b** vs. **ab**).

From the computed sums of the stickiness quotients $y_{ijk.}$ the contrasts and the factorial effects can be calculated according to Equation (1) and (2) (see Chapter 2.4), where *n* is three (replicate tests). Table 4.3 shows the results of the evaluated contrasts, factorial effects and also the calculation of the sum of squares, which are necessary for the further analysis of variances to verify the significance of each factorial effect.

Table 4.2: The stickiness quotient S/R results of the performed design of experiments with systematically varying of the test parameters, which is indicated in the character of the treatment combination; A … Compressive force (-5 / -50 N), B … Hold-time at compressive force (1 / 180 s), C … Haul-off speed (10 / 100 mm/s) ➔ **(1)** = all factors at low level; **abc** = all factors at high level and e.g., **c** = haul-off speed at high level, compressive force and hold-time at low level; Material: N.

	replicate tests n					
	1	*2*	*3*	*mean*		
Test#	**S/R**	**S/R**	**S/R**	**S/R**	**$y_{ijk.}$ Σ**	**Treatment Combination**
/	N	N	N	--	N	/
1	0.52	0.52	0.51	**0.52**	**1.55**	**(1)**
10	0.46	0.46	0.43	**0.45**	**1.35**	**c**
5	0.56	0.55	0.57	**0.56**	**1.68**	**b**
7	0.41	0.43	0.42	**0.42**	**1.26**	**bc**
8	1.06	0.89	0.83	**0.93**	**2.78**	**a**
6	0.83	0.82	0.82	**0.82**	**2.47**	**ac**
4	0.93	0.95	0.97	**0.95**	**2.85**	**ab**
2	1.64	1.54	1.53	**1.57**	**4.71**	**abc**

Table 4.3: The calculated contrasts, factorial effects and the sum of squares from the results of the according to the Equations in Chapter 2.4.

Source of Variation	Contrast	Factor Effect	Sum of Squares
A	6.97	**0.58**	2.02
B	2.35	**0.20**	0.23
C	0.93	**0.08**	0.04
AB	2.27	**0.19**	0.21
AC	2.17	**0.18**	0.20
BC	1.95	**0.16**	0.16
ABC	2.39	**0.20**	0.24

The factorial effect gives the change of the response value, if a factor or more factors would change from the center level (average of high and low level) to the high or low level and the other factors remain at their center level. The influence of the factor increases the response value, if the change from the center level is to the high level. From the effects of the factors (see Table 4.3) it is clearly evident that the compressive force (factor A) has the highest influence on the stickiness test (stickiness quotient). An interesting point is that all factors have an increasing influence on the stickiness quotient. The factor C has the lowest effect, and B has the same effect on the

stickiness quotient like ABC (interaction effect). Furthermore, the interactions have all almost the same effects on the response value.

To analyze if the main and interaction effects are significant, an ANOVA including the F test (upper-tail, one-tail critical value) was carried out (procedure see Table 2.2.). Table 4.4 shows the results of the ANOVA with the computed F_0 values. Moreover, the critical value $F_{0.99, 1, 16}$ ($F_{\alpha, (DoFr), abc(n-1)}$) is listed, which should be smaller than the F_0 value to reject the null hypothesis H_0 (factor has no significance on the experiment). So, the trueness of the alternative hypothesis H_1 would be verified (see Chapter 2.4 and Equation (5)).

Table 4.4: The Analysis of Variance (ANOVA) for the 2^3 factorial design according to the procedure in Table 2.2.

Source of Variation	Sum of Squares	Degrees of Freedom	MST Mean Square	MST/MSE F_0	$F_{0.99, 1, 16}$
A	2.02	1	2.02	**856.81**	***> 8.53***
B	0.23	1	0.23	**97.40**	
C	0.04	1	0.04	**15.25**	
AB	0.21	1	0.21	**90.88**	
AC	0.20	1	0.20	**83.05**	
BC	0.16	1	0.16	**67.06**	
ABC	0.24	1	0.24	**100.74**	
Error	0.04	16	0.00236		
Total	3.14	23			

From the performed F test it can be deduced that all main and interaction effects are significant for the response value (stickiness quotient) and so for the stickiness test. However, the factor A (compressive force) has the highest mean square and F_0 value, and is the most significant factor for the stickiness value. This was also visible in the factorial effects evaluation, where the factor A had the highest influence on the result by changing this factor from the center level to the high or low level and remaining the other factors at their center level. Since the significance of the factor B and C is much lower as in case of factor A, the standardized test parameters for the further investigations were defined as factor A at high level, B and C at the center level:

- Compressive force, F = -50 N
- Hold-time, t_H = 91 s
- Haul-off speed, v = 55 mm/s

Figure 4.2 shows the graphs of three test runs measured on the aluminum reference's surface with the optimal parameter set-up of the tensile machine, where the x-axis and the y-axis are the displacement of the die tip and the measured force, respectively. Moreover, the standard deviation of the average stickiness force is illustrated in Figure 4.2.

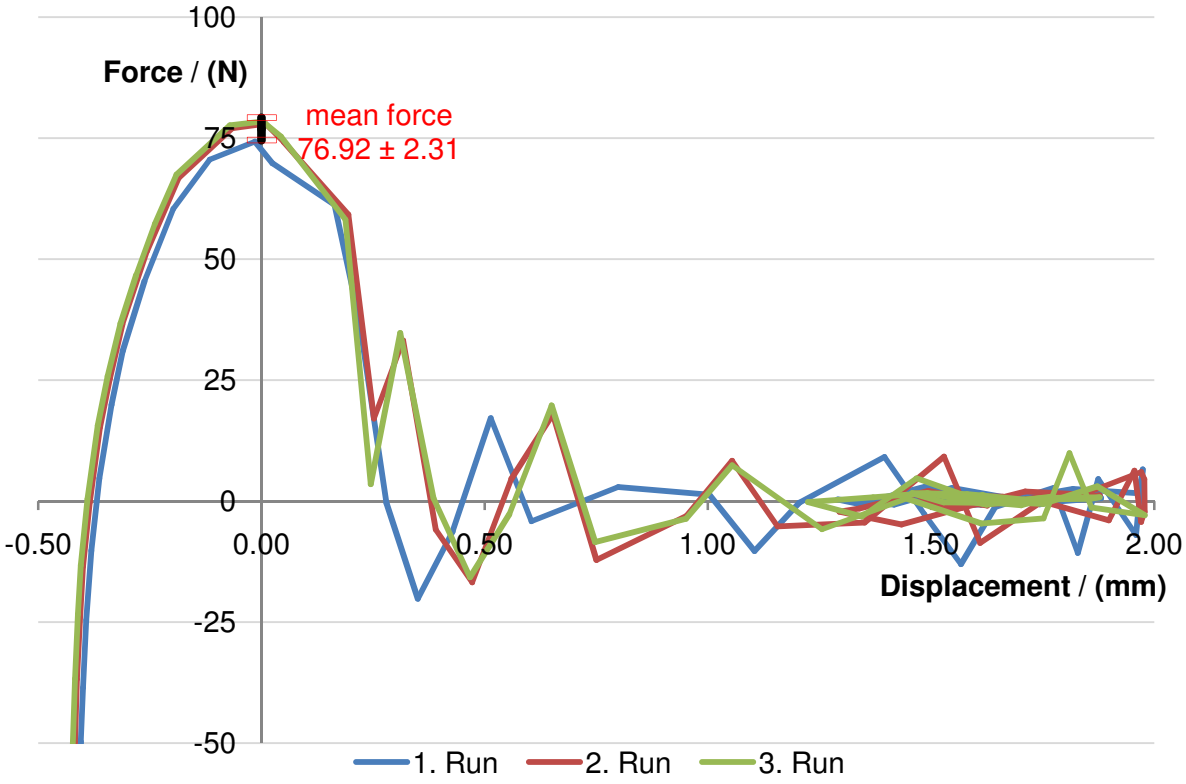

Figure 4.2: Three graphs of the measured stickiness forces of the reference aluminum with one elastomer (cleaned with acetone) to show the reproducibility of the stickiness test. The test parameters were defined as the optimal test parameters (see Chapter 3.4.2); Material: aluminum (reference).

These graphs are an example for the measured reference material aluminum, which was measured previous to the specimen. For both the reference and the specimen the same acetone cleaned elastomer was used. Although, the stickiness test is com-

pletely validated in terms of standardized testing condition. Now the reliability of the stickiness test is to be clarified in the haptic panel.

4.1.3 Haptic Panel

Figure 4.3 shows the comparative results of the stickiness test and Haptic panel for the two performed sessions. The sessions were organized on November 19th (Panel 1) and December 17th (Panel 2), where 16 and 12 testers assessed the surfaces, respectively.

Figure 4.4 illustrates the results of the comparison of significance between pairs according to the Friedman-Test (see Chapter 3.5). The higher the sum of the ranks, the stickier the material's surface.

The stickiness test and the haptic panel assessment were performed on the reverse side of the specimens. Since both measurement and assessment were carried out on the same surface, it was assumed that the influences were also the same. From the stickiness quotient results of Panel 1 the materials can be ranked as EbS, SilA, N, and OleA regarding to the increasing sticky touch of the surface. From the Haptic panel ranks' statistical comparison of pairs (see Figure 4.4) it can be deduced, that there is no significant difference between the next neighbors within the ranking. There are only significant differences between each second material of the rank. The results of Panel 2 show a similar ranking. This time, the correlation between the stickiness test and the Haptic panel was better, and also the assessed stickiness was more significant according to Friedman-Test. Although, there is still no significant difference between the next neighbors of the Haptic panel ranks.

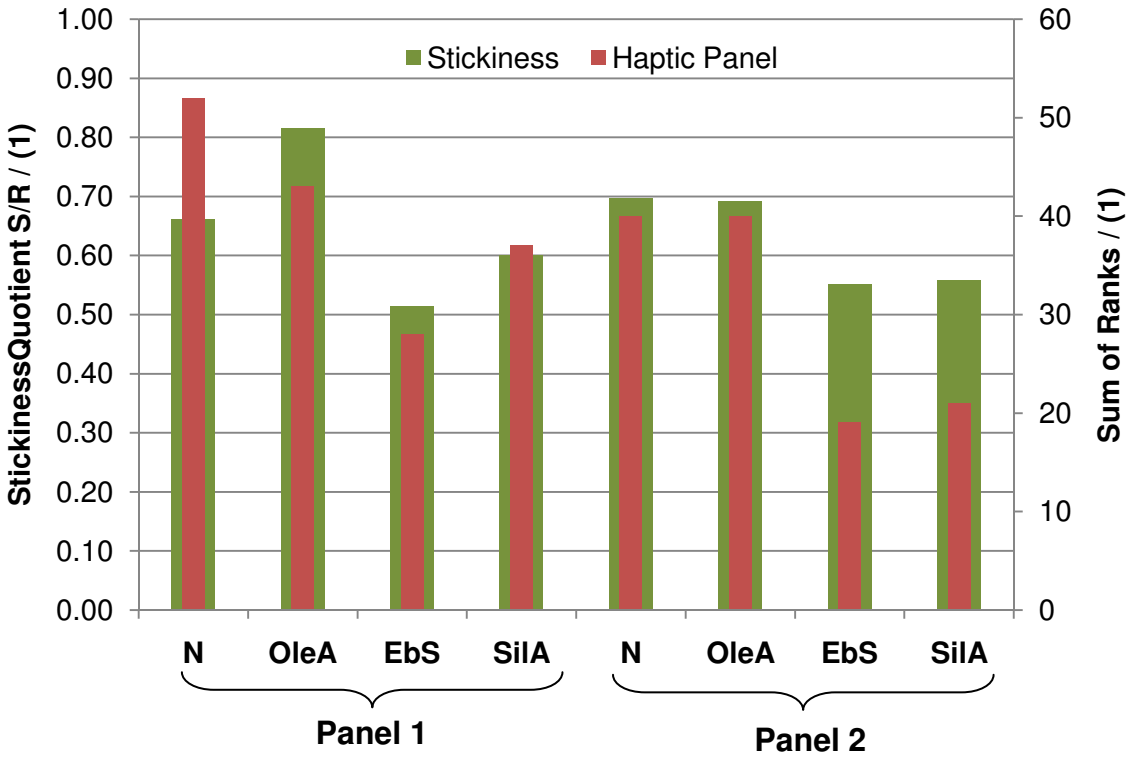

Figure 4.3: Illustration of the comparison of the stickiness quotient S/R (left y-axis) and the results of the Haptic panel specified as sum of ranks (right y-axis) for the investigated materials; high to low sticky touch are ranked from 4 to 1, respectively; 2 sessions were organized: **19.11 ➔ 16 tester**, **17.12 ➔ 12 tester**.

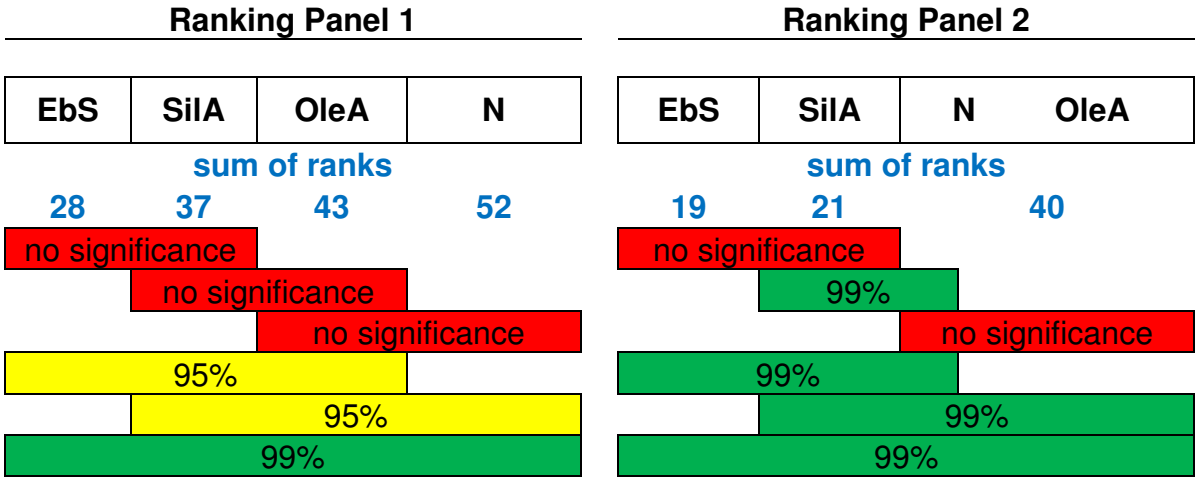

Figure 4.4: Comparisons of significance between pairs according to Friedman-Test for the Haptic panel sessions: **Panel 1 ➔ 16 tester**, **Panel 2 ➔ 12 tester**.

These results justify the reliability of the stickiness test methodology for a comparative testing of stickiness. Although, the test has its limits, which is approximately in the range of the human sense of touch (e.g., results of N and OleA). The verification

of stickiness by the stickiness test is almost the same way like by touching. So, the test is a copy of the natural process of touching with another material than human skin. Since the results of this comparative experiment give a very good correlation between the elastomer die tip and the human skin of different testers, the stickiness test is a less time consuming, objective, and easy to implement methodology. Furthermore, it is convenient to screen a series of materials to find out the best of them with the desired surface properties.

4.2 Scratch visibility

Figure 4.5 shows the results of the scratch test, where the change of lightness ΔL* has been determined as a measure for scratch visibility, after different Kalahari weathering intervals. The scratch visibility gives a qualitative indication of the material's scratch resistance.

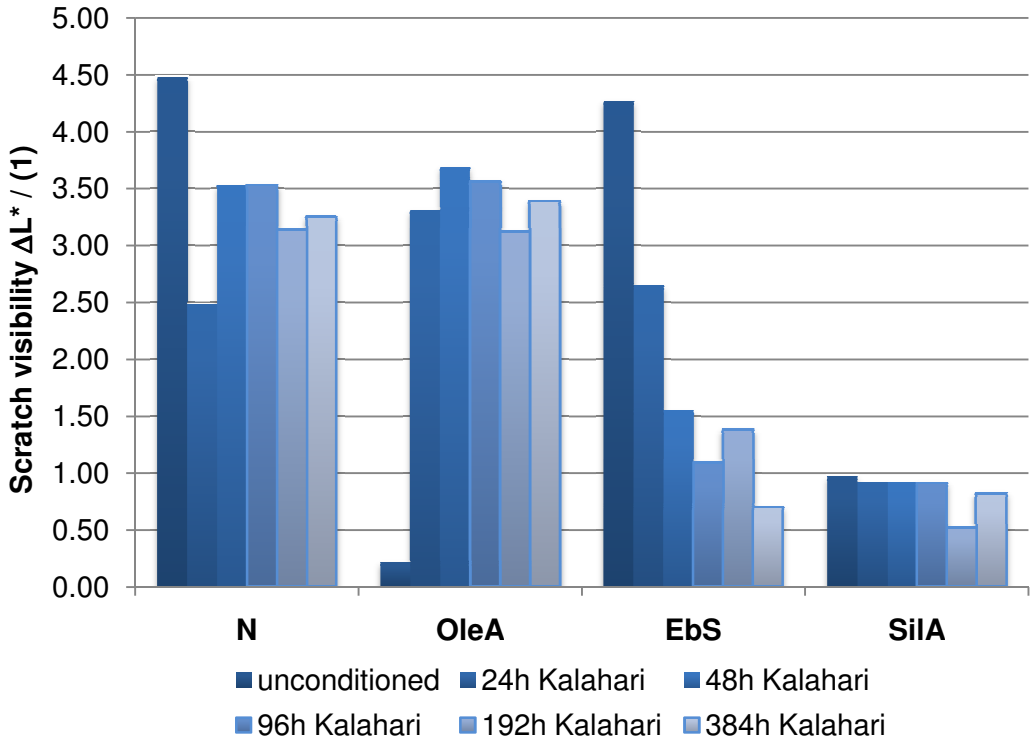

Figure 4.5: Illustration of the scratch visibility, which is measured as change in lightness ΔL*, for the materials after different intervals of Xenon arc light irradiation.

From the scratch visibility results it can be deduced that the material N has the worst scratch performance both in the unconditioned state and in the conditioned state (af-

ter weathering). In fact, the first and second value are higher and lower than the other measured ΔL* values, respectively. Unfortunately, for each condition there was only one specimen available and so it was not possible to repeat and verify the results of these experiments. Despite these, the results of material N show no significant scratch resistance at all, which is a consequence of the filler content and the absence of slip agents. Thus, the results are reflecting the pure surface property of the TPO-materials. This is also confirmed by the scratch visibility properties of the OleA and EbS formulations, which represent the migrating slip agent systems. In the unconditioned state, OleA and EbS show the best and the worst ΔL*, respectively. During weathering, the OleA formulation becomes an almost constant scratch visibility value, which is similar to the scratch visibility of the material N. So, there is no more scratch resistance improving effect of oleamid evident on the materials surface after approximately 48 h. Furthermore, the results of the material OleA indicate that the concentration of the slip agent is also consumed in the bulk material. If there would be still sufficient amount of slip agent in the material, it would migrate out of the bulk to the surface and so reduce the scratch visibility values over the weathering time. On the other hand, the EbS material shows reducing scratch visibility with increasing time of UV exposure. So, this additive needs more time to initiate the diffusion from the bulk to the surface of the material. The different migrating nature of oleamid and ethylene-bis-stearamid is caused mainly by their different molar mass. Oleamid ($C_{18}H_{35}NO$) and ethylene-bis-stearamid ($C_{38}H_{76}N_2O_2$) have a molar mass of 281 g/mol and 593 g/mol, respectively. Although, the concentration of ethylene-bis-stearamide is higher than of oleamide (see Table 3.1) and so the rate of diffusion should be higher. This is also limited by the two times higher molar mass of ethylene-bis-stearamid, which affect the diffusion rate in an opposed manner. The non-migrating additive based on polysiloxane – material SilA – shows, as expected, a constant scratch resistance performance of the material. A decrease of ΔL* after approximately 192 h is visible, which is probably a little migrating effect to the surface, despite their non-migrating nature.

To sum up, it can be noticed that the silicone based additive has the best scratch visibility performance in this comparison. The oleamid additive gives excellent scratch visibility properties only in the unconditioned state to the TPO. A contrary situation is

apparent for TPOs containing ethylene-bis-stearamid. They give the best results after relatively long weathering. The neat material N has the worst performance in every conditioning states of the material.

4.3 Stickiness*Quotient*

Figure 4.6 illustrates the results of the stickiness test, where the stickiness quotient has been determined as a measure for the sticky touch of the surfaces, after different Kalahari weathering intervals. The stickiness quotient S/R is defined as the specimen's stickiness force divided by the reference's stickiness force (see Equation (8)). Furthermore, the higher the quotient, the stickier the surface, is the way to interpret this value.

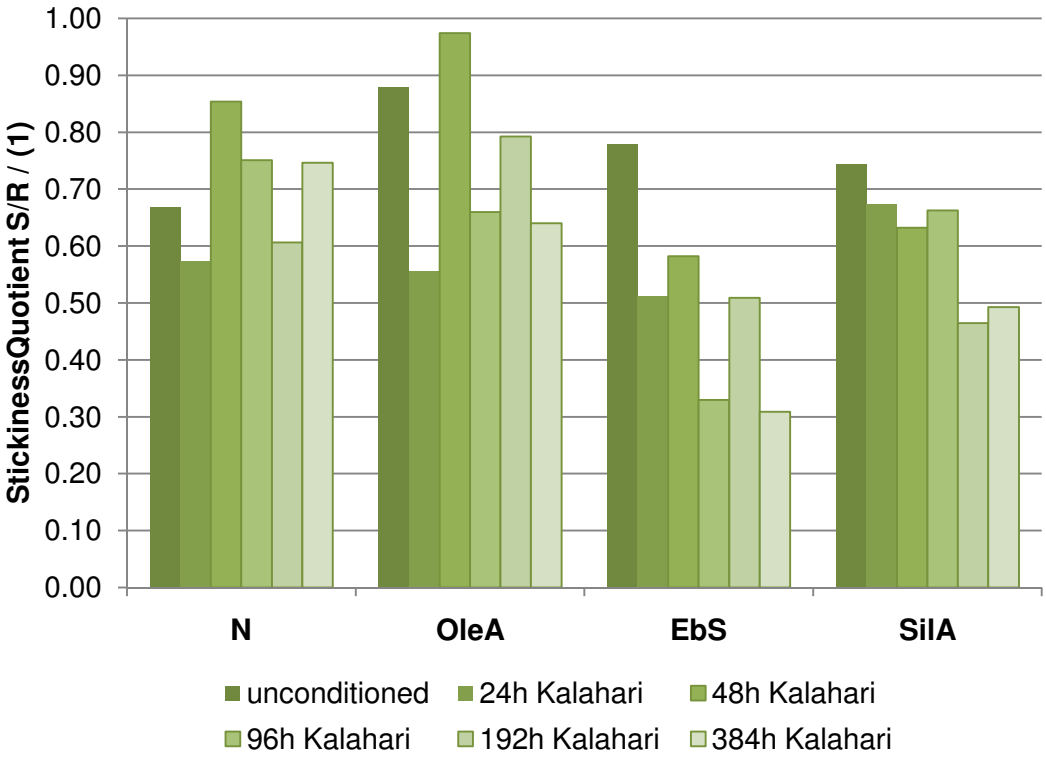

Figure 4.6: Illustration of the stickiness quotient S/R for the TPO materials after different intervals of Xenon arc light irradiating.

The first interesting point is that the elastomer die tip (see Chapter 3.4.1) is better adhesive to the reference aluminum plaque than to the TPO surfaces. This fact does not affect the further interpretation of the results, since the stickiness test is a comparative test methodology, where the stickiness is evaluated relatively to the refer-

ence for all materials. For material N and OleA there is no clear tendency visible from the results of the stickiness quotient. They are apparently fluctuating over the weathering time and there are no significant differences of the results, which mean, they are similar sticky on their surfaces. The EbS material shows a similar decreasing tendency like the ΔL* results. This means, that with increasing migration of the slip agent ethylene-bis-stearamid, the stickiness is decreasing. Also the results of SilA material give a similar tendency like their ΔL* results. The decrease from the values of 96 h to 192 h weathering is more distinct as compared to the ΔL* results.

It has been expected that there are big differences between the neat material N and the materials with the migrating additives. Furthermore, the silicone based additive gives also higher stickiness quotients than expected. These expectations would follow from the hypothesis that stickiness is caused by the migrating slip agents.

4.4 Stickiness*Quotient* vs. Scratch visibility

To compare in detail the stickiness and scratch properties of the surfaces in Figure 4.7 and Figure 4.8 there are illustrated the results of the unconditioned material and the material after 48 h weathering, respectively.

From the results of the unconditioned material (see Figure 4.7) it would be deduced that with increasing scratch visibility (OleA, SilA, and N) the stickiness is decreasing. This relationship between stickiness and scratch behavior is not valid for the material with ethylene-bis-stearamid. If the results of the material after 48 h weathering (see Figure 4.8) are taken into account, the situation is totally different. After this material conditioning the scratch visibility of material N and OleA are almost the same, but the stickiness quotient of OleA is higher. Material SilA has no significant change in scratch visibility after weathering, but the stickiness quotient is decreased. The behavior of material EbS is very interesting regarding to the observation that a reduction in scratch visibility from 4.27 to 1.55 is accompanied by a decrease in stickiness from 0.78 to 0.58.

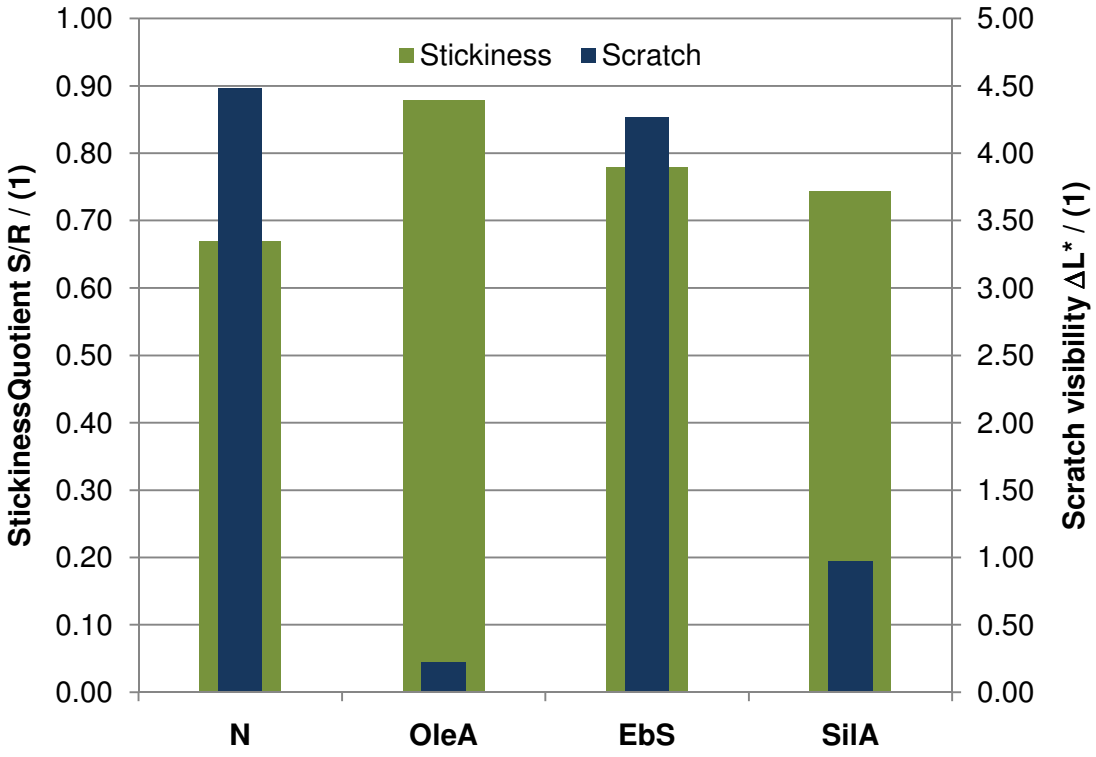

Figure 4.7: Illustration of the comparison of stickiness quotient S/R (left y-axis) and scratch visibility (right y-axis) for the **unconditioned** materials.

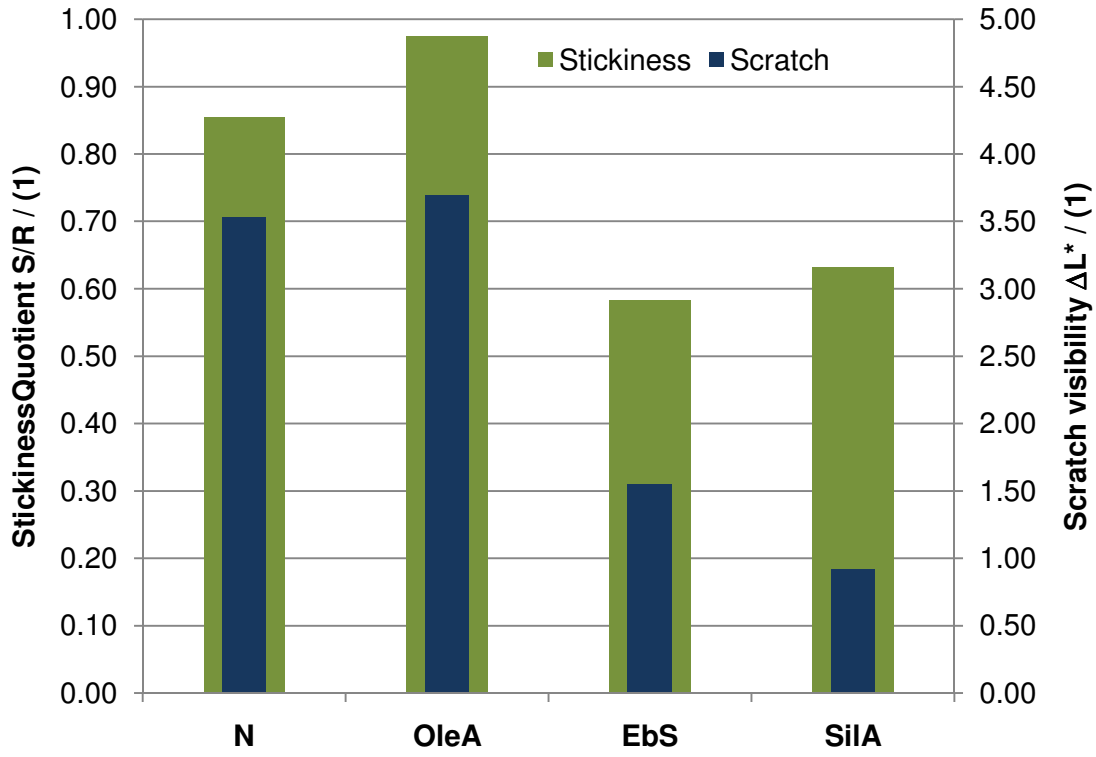

Figure 4.8: Illustration of the comparison of stickiness quotient S/R (left y-axis) and scratch visibility (right y-axis) for the materials after **48 h Kalahari** weathering.

From this characterization of the materials it can be deduced that the slip agents are not the main reason for the occurrence of stickiness on TPO surfaces. This is clearly visible in the results for the UV irradiated materials. The material N – without slip agents – has a similar stickiness quotient like material OleA and higher than the materials EbS and SilA (see Figure 4.6). Furthermore, the material N shows a tendency to increase stickiness during weathering time, but there is no slip agent responsible for this. On the other hand, the material EbS apparently decreases both the stickiness and the scratch visibility during weathering and so with migration of ethylene-bis-stearamid. Hence, the hypothesis that the slip agents are responsible for the occurrence of stickiness, which has been the first impression of the whole stickiness issue, does not fit to the verified results. A possible explanation for the sticky touch of TPO surfaces, especially of the neat material N, might be the antioxidants and the UV stabilizer additives. Since the same base formulation (e.g., antioxidants, UV stabilizer etc.) was used for all investigated materials, it should influence also the other materials in a similar way. However, there were contradictory results measured, such as material EbS and SilA. Moreover, the interactions between the slip agents and antioxidants as well as UV stabilizer additives were affecting the material's stickiness behavior. Basically, the overall polymer blend constituents are affecting the stickiness, which is also described in literature [2; 3]. Despite those, in the current investigation these herein before mentioned additives were affecting the material N primarily and the other materials at least in an interaction with the slip agents. More precise, this interaction influences the slip agent solubility, and diffusion rate [2].

4.5 Weathering behavior of the materials: Change in lightness and gloss

Figure 4.9 and Figure 4.10 illustrate the results of the Kalahari-Test [23], where the change in lightness and gloss were measured according to PV 3929 [23]. These results represent the aging behavior of the materials. Since the investigated materials were black, it is not useful to measure the change in color. Hence, the shift in lightness and gloss during UV irradiation was used to characterize the aging behavior. The higher the L* value, the lighter the material's surface. The unconditioned materials' gloss values were offset to 100% to see the change during weathering.

Basically, from the values of the L* (see Figure 4.9) it can be seen that there is an increase during UV irradiation time for all materials. In the unconditioned state the L* of material EbS is higher than the other materials, which are almost at the same value. The material OleA increases sharply from the material's unconditioned state to 24 h weathering, followed by a further increase to a maximum after 96 h and then decreases. In a similar way, but not so distinctive, are the results of material SilA. The results of the material EbS have a tendency to increase until 384 h weathering, but between 48 h and 192 h irradiation the L* values are almost the same.

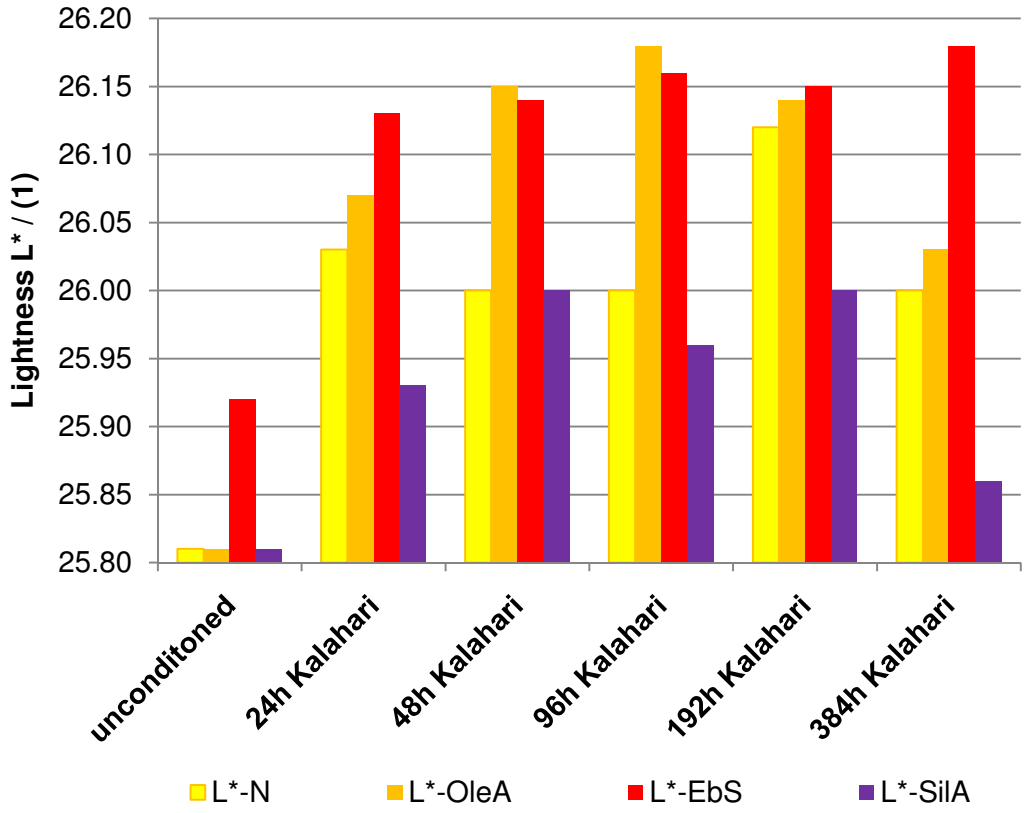

Figure 4.9: Illustration of the lightness L* (y-axis) of the materials after different intervals of Kalahari irradiation.

The gloss results (see Figure 4.10) show an increase over the weathering time for all materials. Basically, the change in gloss is almost the same for all materials. Despite that, the absolute gloss values indicate that EbS has the highest change, followed by N, OleA, and SilA until 192 h Kalahari weathering. After 384 h weathering the rank of change in gloss is N, EbS, SilA, and OleA.

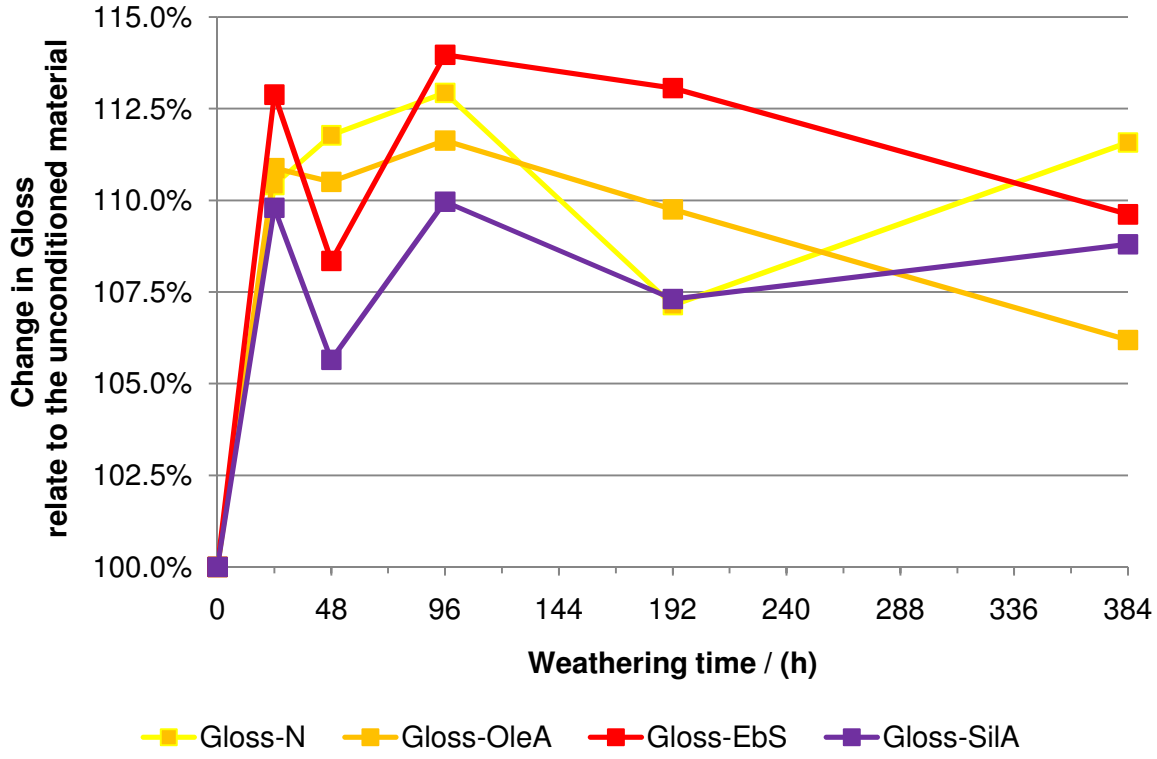

Figure 4.10: Illustration of the change of gloss (y-axis) of the materials related to their unconditioned state.

From these results it can be clearly seen that the different types of slip agents incorporated in the base materials have a significant influence of their aging behavior. The main influencing factors of the aging behavior are post crystallization, and degradation of additives, among other factors.

4.6 FT-IR Spectra

The measured FT-IR spectra of the materials' surfaces are illustrated from Figure 4.11 to Figure 4.15. There are illustrated both the unconditioned materials and the materials after 48 h Kalahari weathering, to see the change of the materials' surfaces. For the further discussion the spectra are focused to the interesting range, where a change of the bands have been evident. The whole spectra are illustrated in the appendix of this thesis (see Chapter 7).

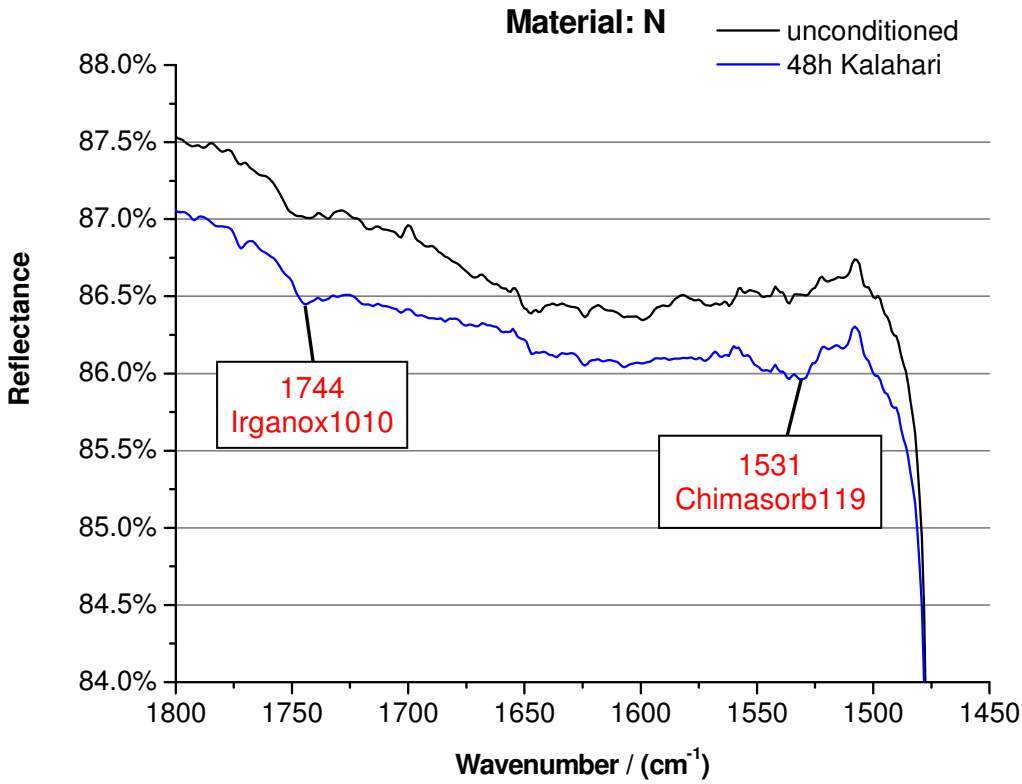

Figure 4.11: The measured FT-IR spectrum of the material N focused between 1450 cm^{-1} and 1800 cm^{-1}; black ➔ unconditioned material's surface, blue ➔ the materials surface after 48 h Kalahari weathering.

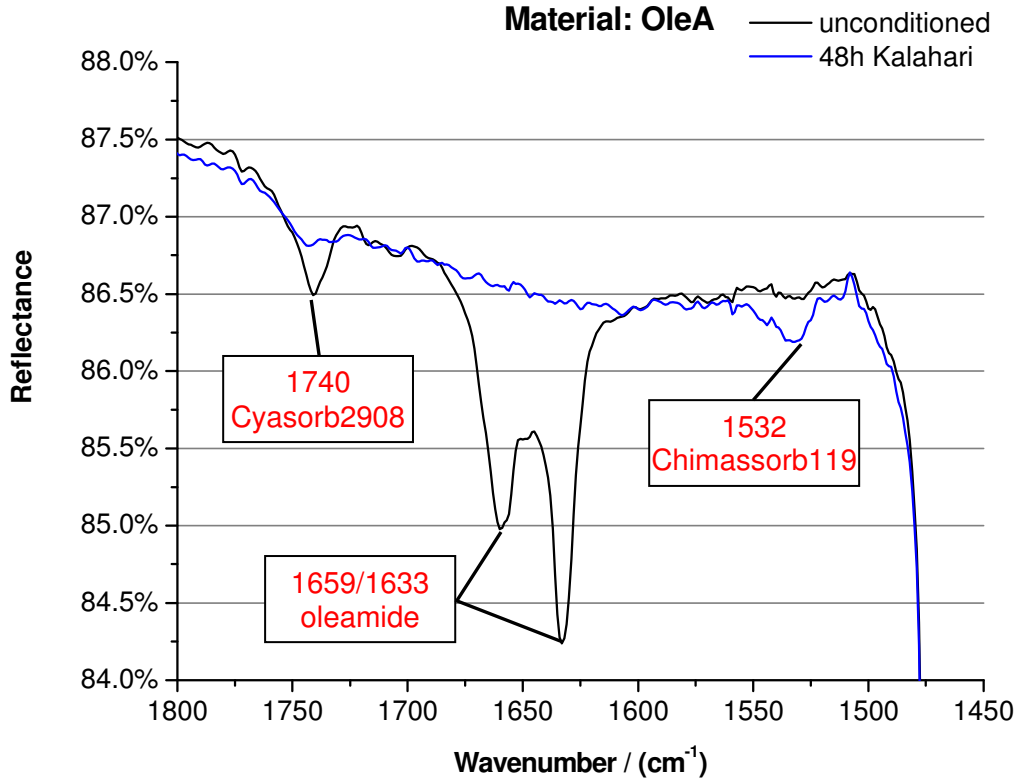

Figure 4.12: The measured FT-IR spectrum of the material OleA focused between 1450 cm^{-1} and 1800 cm^{-1}; black ➔ unconditioned material's surface, blue ➔ the materials surface after 48 h Kalahari weathering.

The material N (see Figure 4.11) shows a shift of the spectrum to lower reflectance during weathering. This is caused by post crystallization of the material. Furthermore, the spectra indicates a slight migration of the antioxidant Irganox 1010 (1744 cm^{-1}) and the UV stabilizer Chimassorb 119 (1531 cm^{-1}) during artificial weathering.

The spectrum of the material OleA (see Figure 4.12) has no significant shift of the spectrum during weathering. Also the migration of the UV stabilizer Chimassorb 119 (1532 cm^{-1}) is visible during weathering. However, the UV stabilizer Cyasorb 2908 (1740 cm^{-1}) is evident on the material's surface only in the unconditioned state. In the weathered state of the surface there is no more Cyasorb 2908 visible in the IR spectrum. The very interesting fact is that the oleamide (1633 cm^{-1} and 1659 cm^{-1}) additive is only on the unconditioned material's surface evident. After 48 h Kalahari weathering there is no more oleamide on the surface. This is also conforming the scratch visibility results. Furthermore, the fact that there is no measureable oleamide on the surface, leads to the assumption that in the bulk material the concentration is also depleted otherwise the oleamide would still migrate to the surface.

The spectrum of material EbS (see Figure 4.13) shows an aging behavior in terms of post crystallization in the range of the material N. The shift is in the same order of magnitude. There is also a migration of the UV stabilizer Chimassorb 119 (1531 cm^{-1}) during weathering visible. Contrary to the material OleA this material shows a migration of the anti-scratch additive ethylene-bis-stearamide (1557 cm^{-1} and 1638 cm^{-1}). The concentration of ethylene-bis-stearamide on the material's surface is higher after 48 h Kalahari weathering. This phenomenon is also conforming to the scratch visibility results, where the scratch visibility decreases with increasing of the weathering time.

The material SilA, which is representing the formulation with the nonmigratory slip agent, shows in Figure 4.14 a shift of the IR spectra during weathering. This shift, which is mainly caused by the post crystallization process, is almost in the same range like the material N. On the unconditioned material's surface a little more of the UV stabilizer Cyasorb 2908 (1739 cm^{-1}) is visible than on the material OleA.

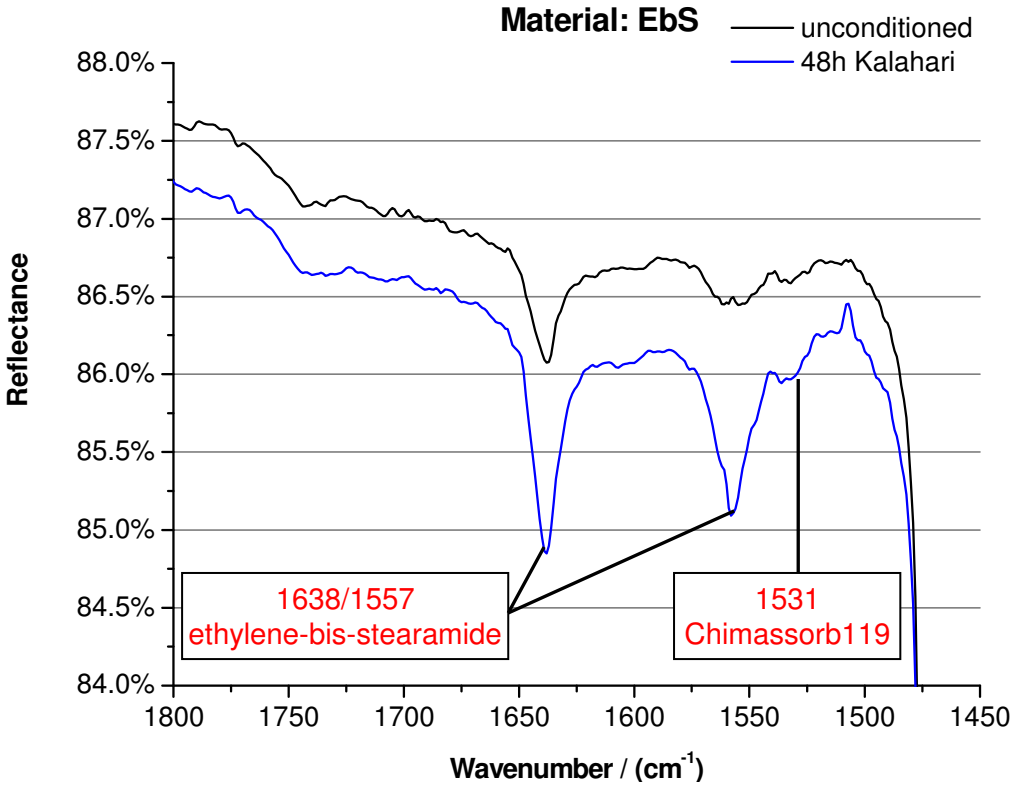

Figure 4.13: The measured FT-IR spectrum of the material EbS focused between 1450 cm^{-1} and 1800 cm^{-1}; black ➔ unconditioned material's surface, blue ➔ the materials surface after 48 h Kalahari weathering.

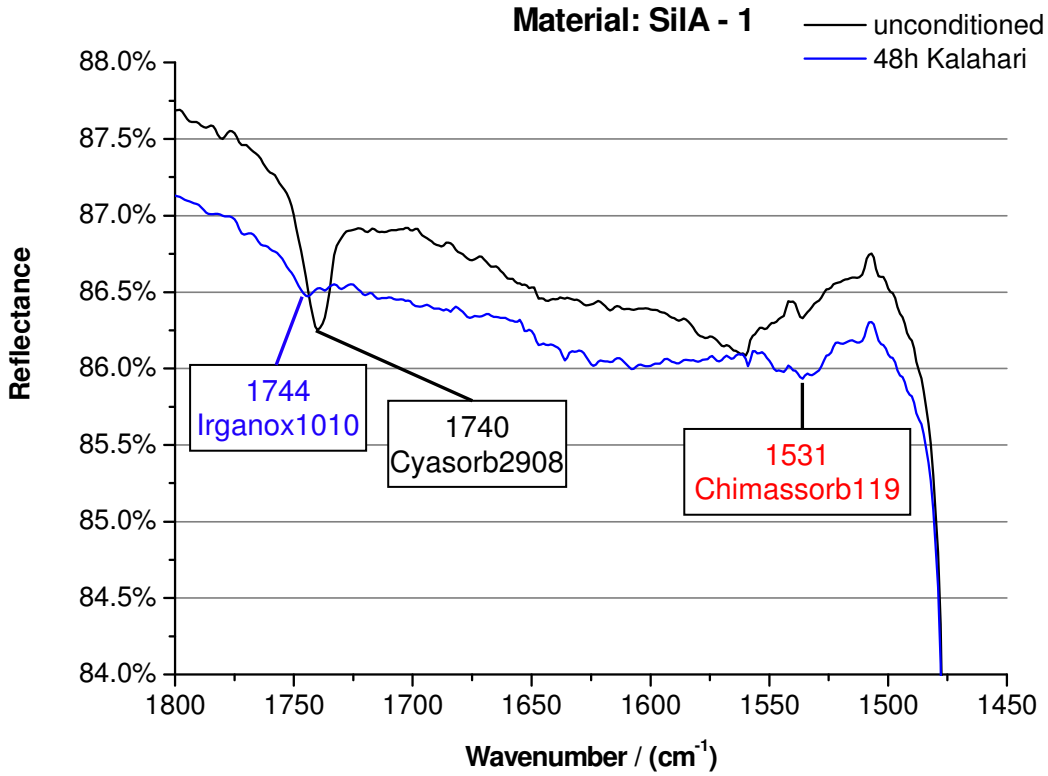

Figure 4.14: The measured FT-IR spectrum of the material SilA focused between 1450 cm^{-1} and 1800 cm^{-1}; black ➔ unconditioned material's surface, blue ➔ the materials surface after 48 h Kalahari weathering.

After 48 h weathering the antioxidants Irganox 1010 (1745 cm^{-1}) and the UV stabilizer Chimassorb 119 (1531 cm^{-1}) are evident on the surface. In Figure 4.15 the range for the silicone band (1260 cm^{-1}) is focused. Despite the nonmigratory nature of the silicone additives, there is a little migration visible. However, this migration is not in the order of magnitude of ethylene-bis-stearamide and so very low. The scratch visibility results also show an almost constant visibility during weathering.

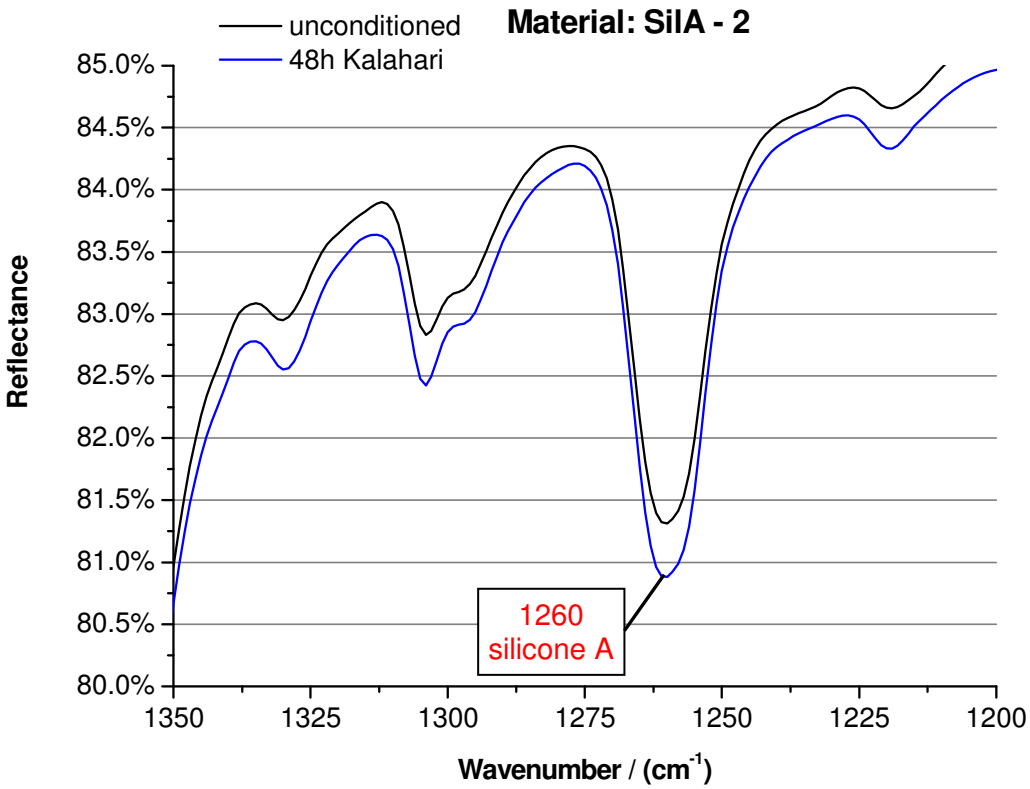

Figure 4.15: The measured FT-IR spectrum of the material SilA focused between 1200 cm^{-1} and 1350 cm^{-1}. black ➔ unconditioned material's surface; blue ➔ the materials surface after 48 h Kalahari weathering;

The measured FT-IR spectra are completely confirming to the scratch visibility results of the investigated materials. It was very surprising that the depletion of the oleamide additive is so extreme. Furthermore, it is also confirmed that the anti-scratch additives are not the main reason of stickiness. Unfortunately, the results give no further indication on the origin of stickiness phenomenon.

5 CONCLUSION AND OUTLOOK

Based on empirical observations it was anticipated that the occurrence of the stickiness phenomenon on PP-compounds' surfaces is linked to the presence of migratory anti-scratch additives. To examine this hypothesis a stickiness test was developed, where the stickiness quotient was established as a measure for the sticky touch of the surface. The influence of different cleaning conditions and testing parameters were verified in terms of reproducibility of the stickiness quotient. To capture the influences of the test parameters a 2^3 factorial design was carried out, where eight experiments were necessary to analyze the significance of parameters (factors). In the current work it was easy to perform all experiments, because the factors were limited to the compressive force of the tensile machine, hold-time at compressive force of the elastomer die tip on the specimen's surface and the haul-off speed from the surface. Furthermore, the experiments were not time consuming and the procedure of the design of experiments gave a systematically way to find the significant parameters. So, the 2^3 factorial design was the fastest way to the desired definition of the test methodology's parameters. The reliability and reproducibility of the stickiness test was shown by both the results of the haptic panel and the standard deviation of the stickiness quotients. Moreover, the haptic panel showed that the limit of the stickiness test was in the order of the human sense of touch. This was as expected, because the stickiness test measures the sticky touch of surfaces in the same way as a human by touching without horizontal movement of the finger. The "die tip" material was an elastomer instead of the human skin. However, it should be mentioned that the pH-value and the moisture of the finger have a significant impact on the human sensation of touch, which was neglected as a first approximation for both the haptic panel testers' fingers and the stickiness test. Despite those influences, the stickiness test is correlating to the human sense of touch and gives an objective measure for stickiness in a very short time.

With the aid of scratch visibility measurement and stickiness test the best additive-surface appearance-cost performance was identified. The material EbS had decreasing stickiness and scratch visibility with increasing duration in the environmental chamber at Kalahari conditions. The best scratch and stickiness performance was

measured for the material SilA, which was expected since this material represents the nonmigratory anti-scratch additives. In contrast to this very stable performance are the high costs of the additive and the higher concentration of additive in the material, which is necessary to have an anti-scratch effect. The last aspect is also caused by their nonmigratory nature.

The results of the scratch visibility measurement were affirmed by the FT-IR spectra analysis. Material OleA had after 48 h Kalahari weathering no more oleamide on the surface and so the scratch behavior was similar to the material without an anti-scratch additive. On the other hand, the migratory nature of the ethylene-bis-stearamide leads to higher concentration during weathering (high temperature) on the material's surface and thus to lower scratch visibility. However, all materials showed also the migration of antioxidants (e.g., Irganox 1010) and/or UV stabilizers (e.g., Chimassorb 119). The UV stabilizer Cyasorb 2908 was evident in the IR spectra of material OleA and SilA in their unconditioned state.

Basically, the hypothesis that only the migratory anti-scratch additives are responsible for the stickiness phenomenon is not true. The best proof were the contradictory results of the material EbS's scratch visibility and stickiness quotient. This material showed with increasing migration of the additive from the bulk to the surface, lower stickiness and as expected lower scratch visibility. So, the reason for the occurrence of stickiness is more a complex interaction of the anti-scratch additives, the antioxidants (e.g., Irganox 1010) and the UV stabilizer (e.g., Chimassorb 119). Unfortunately, the herein investigated model materials had no single antioxidant and UV stabilizer additive. These additives were a compound of different antioxidants and UV stabilizers and so the interpretation of the results according to an interaction of all additives, which would explain the process of the stickiness phenomenon, is not possible.

The last aspect is to be clarified in further studies. Therefore, a series of model materials should be formulated with varying amount and type of antioxidants, UV stabilizers and anti-scratch additives. These materials should be comparative characterized with the scratch visibility and the stickiness test. In addition the FT-IR spectra after

different weathering durations should be measured to deduce a material's formulation-surface property relationship.

6 BIBLIOGRAPHY

[1]. *Additive Approaches to Improving Scratch and Mar Resistance in Automotive Poylolefins.* **Sharma, Ashutosh H., et al.** Michigan : SPE Automotive TPO Global Conference, 2004. URL: http://botkinchemie.com/downloads/spetpo2004_scratch.pdf (2010).

[2]. *New Additive to Improve Scratch Resistance and Reduce Surface Tack for Automotive Applications.* **Huber, Gregor and Solera, Peter.** Lisbon : First Automotive Congress - Plastics in Motion, 2006. URL: http://www.ciba.com/pf/docMDMS.asp?targetlibrary=CHBS_PA_MADS&docnumber=8014 (2010).

[3]. *Technical Approaches to Improving the Scratch Resistance of TPO's Part I: Surface Lubrication.* **Botkin, J.** Michigan : SPE Automotive TPO Global Conference, 2007. URL: http://botkinchemie.com/downloads/BotkinSPETPO2007.pdf (2010).

[4]. **PV1306.** Nichtmetallische Werkstoffe. *Belichtungsprüfung zur Bestimmung der Klebrigkeit an PP-Kunststoffen.* [Volkswagen AG internal standard]. February 2008.

[5]. **Surface Microanalysis Laboratory (LMS), ENSMM.** *Sensotact - The first tactile reference frame.* [Online] http://www.sensotact.com (2010).

[6]. **Drobny, J G.** *Handbook of Thermoplastic Elastomers.* s.l. : Plastics Design Library, 2007.

[7]. *Skin-core morphology and failure of injection-molded specimens of impact-modified polypropylene blends.* **Karger-Kocsis, J and Csikai, I.** 1987, Polymer Engineering and Science, Vol. 27, pp. 241--253.

[8]. *Effects of slip agent and talc surface-treatment on the scratch behavior of thermoplastic olefins.* **Browning, R, et al.** s.l. : Stamford, Conn.: Society of Plastics Engineers,[1965-, 2006, Polymer Engineering and Science, Vol. 46, pp. 601--608.

[9]. **Janet S. S. Wong, Hung-Jue Sue.** Scratch Behavior of Polymers. *Encyclopedia of Polymer Science and Technology.* s.l. : JOHN WILEY & SONS INC, 2003, Vol. 11, pp. 746-765.

[10]. *Scratch and mar resistance of filled polypropylene materials.* **Chu, J, Rumao, L and Coleman, B.** s.l. : Stamford, Conn.: Society of Plastics Engineers, 1998, Polymer Engineering and Science, Vol. 38, pp. 1906--1914.

[11]. **VanLandingham, M R and Giraud, M.** Scratch and Mar Resistance of Polymeric Materials. [ed.] J. W. Martin, R. A. Ryntz and R. A. Dickie. *Service Life Prediction-Challenging the Status Quo.* s.l. : Federation of Societies for Coating Technology, 2005, 23, pp. 305--330. URL: http://slp.nist.gov/pic/pubs.html (2010).

[12]. **ASTM International, D 7027-05.** Standard Test Method for Evaluation of Scratch Resistance of Polymeric Coating and Plastics Using an Instrumented Scratch Machine. 2005.

[13]. *Scratch behavior and material property relationship in polymers.* **Xiang, C, et al.** s.l. : JOHN WILEY & SONS INC, 2001, Journal of Polymer Science Part B Polymer Physics, Vol. 39, pp. 47--59.

[14]. *Understanding of scratch-induced damage mechanisms in polymers.* **Jiang, H, Browning, R and Sue, H J.** s.l. : Elsevier, 2009, Polymer, Vol. 50, pp. 4056--4065.

[15]. *Scratch resistance of mineral-filled polypropylene materials.* **Chu, J, et al.** s.l. : SPE; 1999, 2000, Polymer Engineering and Science, Vol. 40, pp. 944--955.

[16]. **Devries, K. L. and Adams, Daniel O.** Mechanical testing of adhesive joints. [ed.] D. A. Dillard and A. V. Pocius. *Surfaces, Chemistry and Applications: Adhesion Science and Engineering - I (The Mechanics of Adhesion).* s.l. : Elsevier Science B. V., 2002, 6, pp. 193-234.

[17]. **ASTM International, D3354.** Standard Test Method for Blocking Load of Plastic Film by the Parallel Plate Method. November 2008.

[18]. **SAE Society of Automotive Engineers, J 1885.** Accelerated Exposure of Automotive Interior Trim Components Using a Controlled Irradiance Water Cooled Xenon-Arc Apparatus. January 2008.

[19]. *Design and analysis of experiments.* **Montgomery, D C and Montgomery, D C.** s.l. : Wiley New York, 1991.

[20]. **Eschmann Textures International, GmbH.** Texture Guide - Get in Touch. *Aesthetics and functionality of textured surfaces.* [Online] URL: http://www.eschmanntextures.de/fileadmin/user_upload/downloads/guide/Textures_Guide_en.pdf (2010).

[21]. **Ciba Specialty, Chemicals.** Product Selection Guide for Powder Coatings. [Online] http://www.ciba.com/powder.pdf (2010).

[22]. **CYTEC INDUSTRIES, INC.** CYASORB UV-2908 light stabilizer. [Online] http://www.cytec.com/specialty-chemicals/pdf/CYASORBUV2908.pdf (2010).

[23]. **PV3929.** Non-Metallic Materials. *Weathering in Dry, Hot Climate.* [Volkswagen AG internal standard]. March 2008.

[24]. **PV3952.** Kunststoff-Innenraum-Bauteile. *Prüfung der Kratzbeständigkeit.* [Volkswagen AG internal standard]. August 2002.

[25]. **DIN, 5033-4.** Colorimetry; spectrophotometric method. July 1992.

[26]. **DIN, 6174.** Colorimetric evaluation of colour coordinates and colour differences according to the approximately uniform CIELAB colour space. November 2007.

[27]. **Lab, Color.** Digital Exposure. *Glossary.* [Online] http://www.digitalexposure.ca/images/lab.jpg (2010).

[28]. **Semperflex, A560.** [Online] http://www.semperflex.com/uploads/tx_AScatalog/files/A560_01.pdf (2010).

[29]. **DIN, 10963.** Sensorische Prüfverfahren. *Rangordnungsprüfung.* November 1997.

[30]. **ISO, 19252.** Plastics - Determination of scratch properties. 2008.

7 APPENDIX

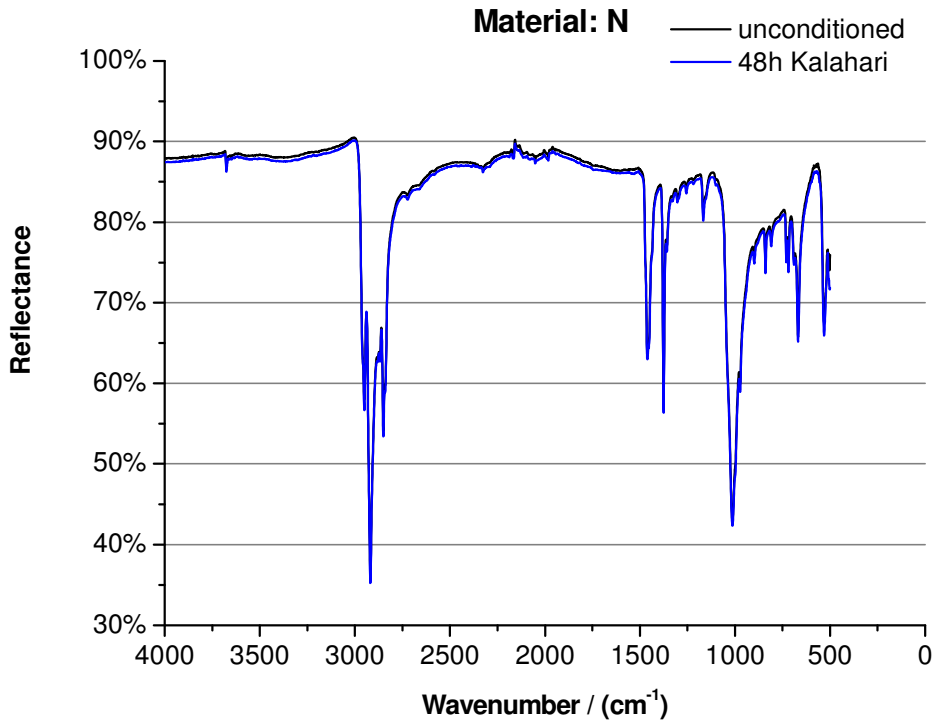

Figure 7.1: Demonstration of the FT-IR spectrum of material N.

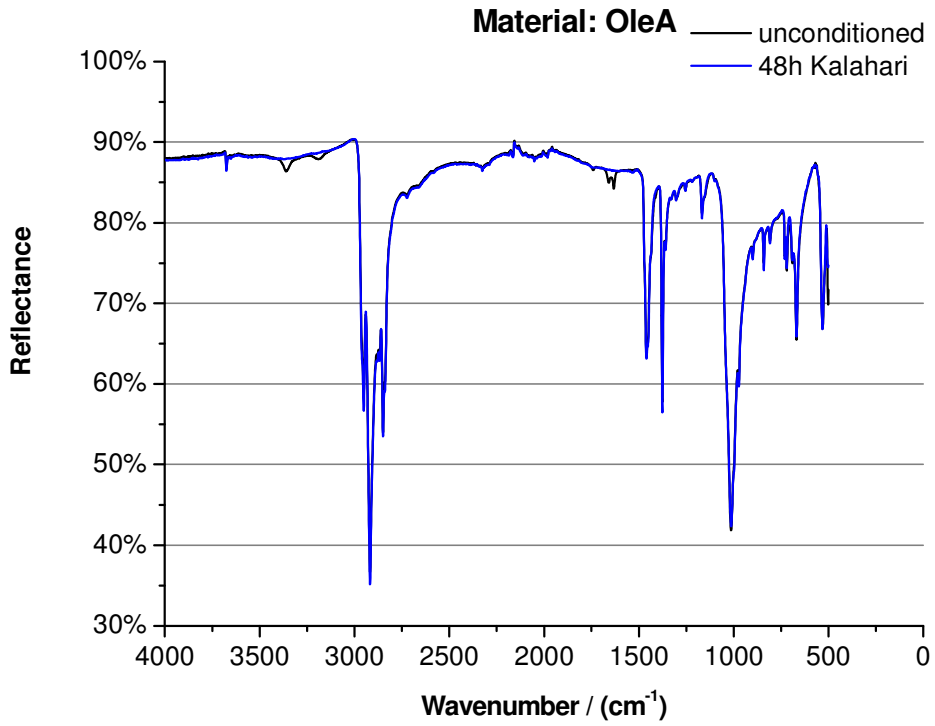

Figure 7.2: Demonstration of the FT-IR spectrum of material OleA.

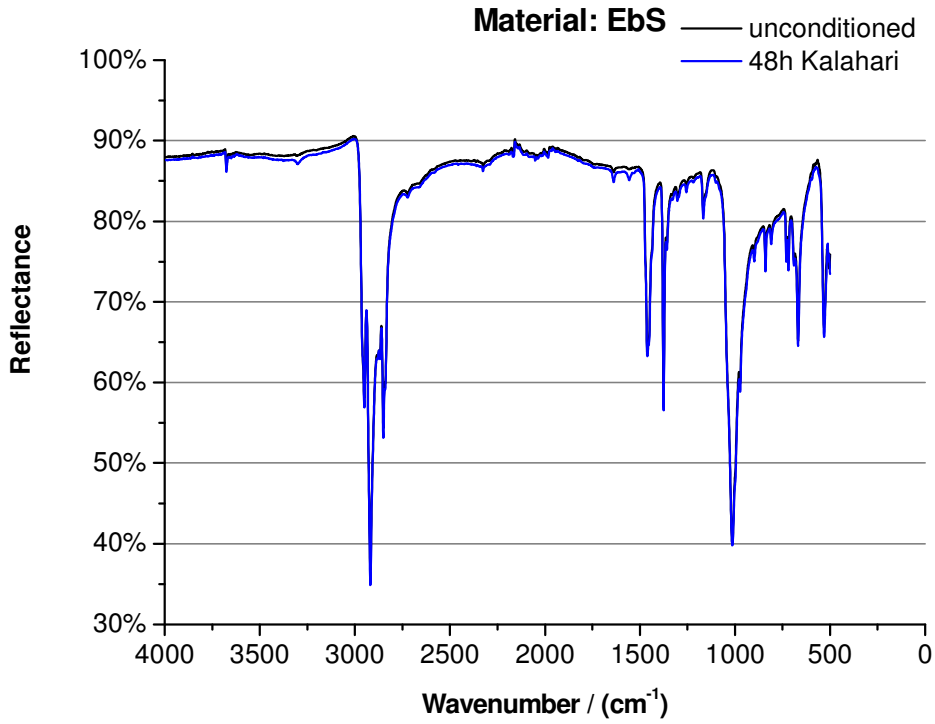

Figure 7.3: Demonstration of the FT-IR spectrum of material EbS.

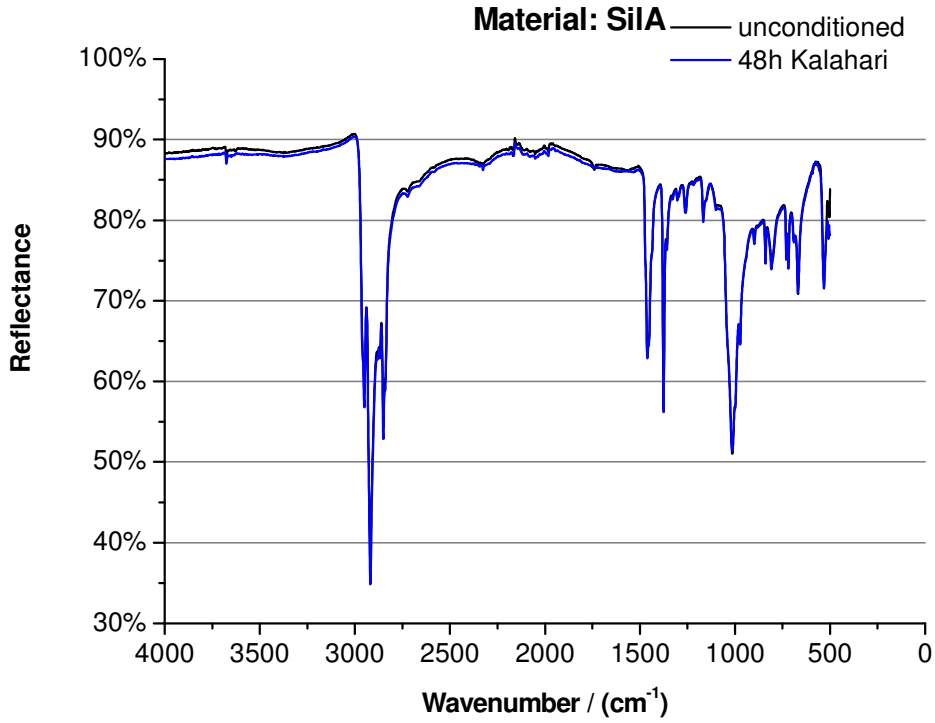

Figure 7.4: Demonstration of the FT-IR spectrum of material SilA.

8 LIST OF FIGURES

9 LIST OF TABLES

AFFIDAVIT

I declare in lieu of oath, that I wrote this thesis and performed the associated research myself, using only literature cited in this volume.

_____ _____

Date Signature